IC/99/83
hep-ph/9907423

Identifying the neutrino mass spectrum from a supernova neutrino burst

Amol S. Dighe [1], *Alexei Yu. Smirnov* [2]
The Abdus Salam International Center for Theoretical Physics
34100, Trieste, Italy.

Abstract

We study the role that the future detection of the neutrino burst from a galactic supernova can play in the reconstruction of the neutrino mass spectrum. We consider all possible 3ν mass and flavor spectra which describe the solar and atmospheric neutrino data. For each of these spectra we find the observable effects of the supernova neutrino conversions both in the matter of the star and the earth. We show that studies of the electron neutrino and anineutrino spectra as well as observations of the neutral current effects from supernova will allow us (i) to identify the solar neutrino solution, (ii) to determine the type of mass hierarchy (normal or inverted) and (iii) to probe the mixing $|U_{e3}|^2$ to values as low as $10^{-4} - 10^{-3}$.

[1] amol.dighe@cern.ch
[2] smirnov@ictp.trieste.it

1 Introduction

The reconstruction of the neutrino mass and flavor spectrum is one of the fundamental problems of particle physics. It also has important implications for cosmology and astrophysics. The knowledge of neutrino masses and mixing will allow us to clarify the role of neutrinos in the mechanism of the star explosion and supernova nucleosynthesis.

With the present data on the atmospheric and solar neutrinos, we are taking the first steps in the reconstruction of the spectrum. The SuperKamiokande (SK) results [1] on atmospheric neutrinos, confirmed by the recent SOUDAN [2] and MACRO [3] data, allow us to claim with a high confidence level that the atmospheric neutrinos oscillate. Moreover, the oscillations are due to neutrino masses and the mixing in vacuum. The data also indicates $\nu_\mu \leftrightarrow \nu_\tau$ as the dominant mode. All the existing experimental results can be well described in terms of the $\nu_\mu \leftrightarrow \nu_\tau$ vacuum oscillations with the mass squared difference and the mixing parameters given by [1]

$$|\Delta m^2_{atm}| = (1-8)\cdot 10^{-3}\ \mathrm{eV}^2 \quad , \quad \sin^2 2\theta = 0.8 - 1.0 \quad . \tag{1}$$

There is no compelling evidence that the electron neutrinos participate in the oscillations of atmospheric neutrinos. Moreover, the CHOOZ experiment [4] gives an upper bound on the mixing of ν_e with $\Delta m^2 \sim \Delta m^2_{atm}$:

$$\sin^2 2\theta_e \leq 0.1 \quad \text{for} \quad |\Delta m^2| > 2\cdot 10^{-3}\ \mathrm{eV}^2 \quad . \tag{2}$$

The oscillation interpretation of the atmospheric neutrino data indicates that the solution of the solar neutrino problem is also related to nonzero neutrino masses and mixing. At the moment, however, there are several possible solutions. Moreover, various sorts of data – spectral distortions, day-night effects, seasonal variations – favor different possible solutions. A good desription of all the existing data can be obtained by [5]:

1. the small mixing angle (SMA) MSW solution:

$$\Delta m^2_\odot = (4-10)\cdot 10^{-6}\ \mathrm{eV}^2 \quad , \quad \sin^2 2\theta_\odot = (2-10)\cdot 10^{-3} \quad , \tag{3}$$

2. the large mixing angle (LMA) MSW solution:

$$\Delta m^2_\odot = (1-10)\cdot 10^{-5}\ \mathrm{eV}^2 \quad , \quad \sin^2 2\theta_\odot = 0.7 - 0.95 \quad , \tag{4}$$

3. the vacuum oscillation (VO) solution:

$$\Delta m^2_\odot = \begin{array}{c} (4-6)\cdot 10^{-10}\ \mathrm{eV}^2 \\ (6-8)\cdot 10^{-11}\ \mathrm{eV}^2 \end{array} \quad , \quad \sin^2 2\theta_\odot = 0.8 - 1.0 \quad . \tag{5}$$

Some other possibilities are also not excluded – *e.g.* the LOW MSW solution with $\Delta m^2 \sim (0.5-2)\cdot 10^{-7}\ \mathrm{eV}^2$ and $\sin^2 2\theta_\odot = 0.9 - 1.0$ (see [5, 6]). Results from future

experiments with the existing and new detectors will remove this ambiguity, thus identifying the correct solution to the solar neutrino problem.

Another evidence for the neutrino oscillations follows from the LSND results [7], which are not confirmed, but also not excluded by the KARMEN experiment [8]. The LSND results cannot be reconciled with the solutions of the atmospheric and solar neutrino problems in the context of only three known neutrinos, thus requiring the introduction of sterile neutrinos. [9]. In this paper, we shall consider only the mixing between the known three neutrinos (spectra with sterile neutrinos will be discussed elsewhere).

The atmospheric and solar neutrino results ([1]-[3], [5]) as well as the existing bounds from the other oscillation experiments and the $\beta\beta_{0\nu}$ searches lead to several possible spectra of neutrino masses and mixing. The ambiguity is related to (i) the unidentified solution of the solar neutrino problem (ii) unknown mixing of ν_e in the third mass eigenstate which is described by the matrix element U_{e3} (iii) type of hierarchy (normal or inverted) which is related to the mass of the third mass eigenstste (whether it is the lightest or the heaviest one). The absolute scale of mass is also unknown, however this cannot be established from the oscillation phenomena.

In this paper, we reconsider the effects of oscillations on supernova neutrinos. With the existing data on neutrino masses and mixing, we can sharpen the predictions of the oscillation effects in the supernova neutrinos. On the other hand, we clarify the extent to which the studies of supernova neutrinos can contribute to the reconstruction of the neutrino masses and flavor spectrum. We will show that three ambiguities mentioned above can in principle be resolved by supernova data.

The effects of neutrino mixing on the neutrino fluxes from the supernova have been extensively discussed in the context of 2ν mixing. For a wide range of mixing parameters ($\Delta m^2 \lesssim 10^4$ eV^2), the neutrinos encounter their MSW resonance densities inside the star, hence the studies of resonant neutrino conversions inside the star [10]-[12] are crucial. For very low values of Δm^2 (*e.g.* $\Delta m^2 \lesssim 10^{-14}$ eV^2), the vacuum oscillations on the way from the star to the earth need to be taken into account [13, 14]. In the presence of a strong magnetic field, the spin-flip effects become important [15]: the spin-flavor precession [16] and resonant spin-flavor conversions [17] may affect the observed neutrino fluxes. If sterile neutrinos are involved in the neutrino conversions, they may enable the r-process nucleosynthesis [18].

The effects of the neutrino conversions can be observed through, *e.g.* (i) the disappearance (partial or complete) of the neutronization peak; (ii) the interchange of original spectra and the appearance of a hard ν_e spectrum; (iii) distortions of the ν_e energy spectrum; (iv) modification of the $\bar{\nu}_e$ spectrum (in particular, the effects of large lepton mixing on the $\bar{\nu}_e$ spectrum have been extensively studied [19]); (v) earth matter effects. The observation of the neutrino burst from SN1987A [20] has already given bounds on the large mixing of active neutrinos ([11, 12],[19]-[22]) and on the mixing of ν_e with sterile neutrinos [23].

The main features of transitions of supernova neutrinos in the case of 3ν mixing ([22],[24]-[30]) can be understood in terms of the 2ν mixing. The system has two

resonances[3] Under the assumptions of mass hierarchy and smallness of mixing, the dynamics of the two level crossings splits. As a result, the factorization of probabilities occurs [24, 25]. In the presence of sterile neutrinos, multi-level conversions take place [28, 31], which may be interpreted in terms of the constituent 2ν conversions for small mixing angles and Δm^2 hierarchy [9].

In this paper, we study the conversions of supernova neutrinos in the 3ν context, taking into account the recent results on the neutrino masses and mixing. We consider the effects for all possible schemes of neutrino masses and mixing which explain the atmospheric and solar neutrino data. For each scheme, we find the modifications of (i) the neutronization peak (ii) the ν_e energy spectrum and (iii) the $\bar{\nu}_e$ energy spectrum, which can be observed directly. We also determine the spectrum of the non-electron neutrinos which can in principle be studied by neutral current interactions in reactions with different energy thresholds.

The paper is organized as follows. In Sec. II we describe the features of initial neutrino fluxes from the supernova and the dynamics of neutrino conversion on their way out to the surface of the star. In Sec. III, we derive general expressions for the transition probabilities for the schemes with normal mass hierarchy. We also calculate the earth matter effects on the neutrino spectra. In Sec. IV, we find the final neutrino spectra at detectors for the schemes with the normal mass hierarchy. In Sec. V, we perform similar studies for the schemes with the inverted mass hierarchy. In Sec. VI, we discuss the observable signals and the signatures of various mixing schemes In Sec. VII, comparing results for various schemes we conclude about the possibility to discriminate the schemes by future observations of neutrino bursts from a galactic supernova.

2 Mass spectra, fluxes and dynamics of conversion

In this section, the generic properties of the initial neutrino fluxes will be summarized. We identify the neutrino mass and mixing parameters relevant for the supernova neutrino conversions, and consider main aspects of dynamics of neutrino conversion inside the star: the transition regions, the factorization of dynamics and adiabaticity. Finally, we construct the level crossing schemes for the normal and the inverted mass hierarchy.

2.1 Neutrino fluxes

In what follows we will summarize the generic features of the original fluxes which do not depend on the model and the parameters of the star. The deviations from these features will testify for neutrino conversions.

[3]The radiative corrections to m_{ν_μ} and m_{ν_τ} imply the existence of one more resonance between the two non-electron neutrinos, but since the two non-electron neutrinos cannot be distinguished at the detector, the conversions between them do not affect the observations. See sec. 2.6.

1. Flavor of the neutronization peak. During first few milliseconds of the neutrino burst from a supernova, the signal is expected to be dominated by the ν_e, which are produced by the electron capture on protons and nuclei while the shock wave passes through the neutrinosphere [32]. Since the original flux is ν_e, the final observed fluxes give a direct measurement of the extent of conversion of ν_e into the other neutrino species.

2. Inequalities of average energies of the spectra. Since ν_e interact more strongly with matter than the other species, their effective neutrinosphere is outside the neutrinospheres of the other species and hence they have a lower average energy than $\bar{\nu}_e$ and ν_x. The $\bar{\nu}_e$ also interact via charged current, but the cross section is smaller, so their average energy is more than that of the ν_e, but less than that of ν_x.

$$\langle E^0_{\nu_e} \rangle < \langle E^0_{\bar{\nu}_e} \rangle < \langle E^0_{\nu_x} \rangle \quad . \tag{6}$$

Here subscript 0 refers to the original spectra. The neutrino conversion changes inequalities (6).

3. The pinched spectra during the cooling stage. Let F^0_e and $F^0_{\bar{e}}$ be the original fluxes of ν_e and $\bar{\nu}_e$ respectively, produced at the cooling stage. The "non-electron" neutrinos $(\nu_\mu, \nu_\tau, \bar{\nu}_\mu, \bar{\nu}_\tau)$ have the same neutral current interactions inside the supernova, and their original fluxes are expected to be approximately equal[4]. In what follows we will neglect the difference of fluxes. We will denote these four neutrino species collectively as ν_x and the original flux of each of them as F^0_x.

The spectra of neutrinos from the cooling stage are not exactly thermal. Since the neutrino interaction cross-section increases with energy, even for the same species of neutrinos, the effective neutrinosphere radius increases with increasing energies. Then, even if the neutrinos at their respective neutrinospheres are in thermal equilibrium with the matter, the spectrum gets "pinched", i.e. depleted at the higher as well as the lower end of energies in comparison with thermal spectrum. (See Fig. 1 for an illustration.) It can be shown that pinching of the instantaneous spectrum is the consequence of the following two facts: (i) the temperature inside the supernova decreases with increasing radius and (ii) the density decreases faster than $1/r$ [34]. The pinching of the instantaneous spectrum can be extended to the pinching of the time-integrated spectrum as long as the time variation of the average energy of the spectrum is small. Numerical simulations of the neutrino spectra confirm the pinching of spectra [35, 36].

One way to parametrize the pinched neutrino spectra is to introduce an effective temperature T_i and an effective degeneracy parameter η_i (which has the same sign for neutrinos and antineutrinos and cannot be considered as the chemical potential)

[4]The presence of real muons in the central part of the star leads to a nonzero chemical potential of the muon neutrinos and hence to a difference of fluxes [33]. However, in the neutrinosphere with $T \approx 6 - 8$ MeV, the concentration of muons is smaller than 1%.

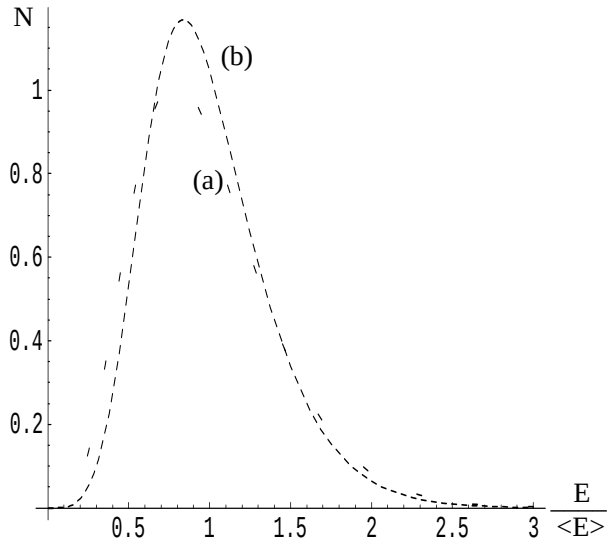

Figure 1: The number of $\nu - N$ charged current events for (a) a thermal spectrum ($T = 3, \eta = 0$) (b) a "pinched" spectrum ($T = 3, \eta = 3$). T and η are the parameters as in Eq. (7). Both the energy resolution function and the lower energy threshold effects have been taken into account. The spectra are normalized to have equal areas.

in the Fermi-Dirac thermal spectrum for each species i:

$$F_i^0(E) \propto \frac{E^2}{Exp(E/T_i - \eta_i) + 1} \quad . \tag{7}$$

For a pinched spectrum, $\eta_i > 0$. The value of η_i is the same for all ν_x species (neutrinos as well as antineutrinos, since they have the same interactions), and are in general different from η_e or $\eta_{\bar{e}}$. The value of η_i need not be constant throughout the cooling stage. Typically,

$$T_e \approx 3 - 4 \text{ MeV} \quad , \quad T_{\bar{e}} \approx 5 - 6 \text{ MeV} \quad , \quad T_x \approx 7 - 9 \text{ MeV} \ . \tag{8}$$

The typical values of η_i are [36, 37]

$$\eta_e \approx 3 - 5 \quad , \quad \eta_{\bar{e}} \approx 2.0 - 2.5 \quad , \quad \eta_x \approx 0 - 2 \quad . \tag{9}$$

Notice that the strongest pinching is expected for the ν_e spectrum. These values, however, are model-dependent and we shall use them only as a guide.

In what follows, we shall calculate the fluxes of electron neutrinos F_e, electron antineutrinos, $F_{\bar{e}}$, and the total flux of the non-electron neutrinos, "$4F_x$" at the Earth detectors.

2.2 Neutrino mass spectra

We consider the system of three active neutrinos $\vec{\nu}_f \equiv (\nu_e, \nu_\mu, \nu_\tau)$ mixed in vacuum, such that

$$\vec{\nu}_f = U\vec{\nu} \quad , \tag{10}$$

where $\vec{\nu} \equiv (\nu_1, \nu_2, \nu_3)$ is the vector of mass eigenstates and

$$U \equiv ||U_{fi}|| \quad , \quad f = e, \mu, \tau, \quad , \quad i = 1, 2, 3 \tag{11}$$

is the mixing matrix. We take

$$\Delta m^2_{32} \equiv m^2_3 - m^2_2 = \Delta m^2_{atm} \quad , \tag{12}$$

so that the oscillations driven by Δm^2_{23} solve the atmospheric neutrino problem. We identify

$$\Delta m^2_{21} \equiv m^2_2 - m^2_1 = \Delta m^2_{\odot} \quad , \tag{13}$$

where $\Delta m^2_{\odot}$ is in one of the regions (SMA, LMA or VO) implied by the solar neutrino data (eqs. 3,4,5).

The key features of the spectra which play an important role in the applications to the supernova neutrinos are:

1. the hierarchy of Δm^2:

$$|\Delta m^2_{32}| \approx |\Delta m^2_{31}| \gg |\Delta m^2_{21}| \quad ; \tag{14}$$

2. the upper bound on Δm^2:

$$|\Delta m^2_{ij}| \lesssim 10^{-2} \text{ eV}^2 \quad . \tag{15}$$

Since ν_μ and ν_τ are indistinguishable in the supernova neutrino studies, the neutrino transitions are determined by the mixings of the electron neutrino only, i.e. by the elements U_{ei} (11) (see sect. 3 for more details). Moreover, the three U_{ei}'s are related by the unitarity condition $\sum |U_{ei}|^2 = 1$, so that only two mixing elements are relevant, and one can use $|U_{e2}|$ and $|U_{e3}|$.

The element U_{e3} is small, as mentioned in the introduction. If $|U_{e3}|^2 \ll 1$, then U_{e2} (and therefore, U_{e1}) can be found from the solar neutrino data:

$$4|U_{e2}|^2|U_{e1}|^2 \approx 4|U_{e2}|^2(1 - |U_{e2}|^2) \approx \sin^2 2\theta_{\odot} \quad , \tag{16}$$

where $\theta_{\odot}$ is the mixing angle determined in the 2ν analysis of the solar neutrino data.

The system is then determined by two pairs of parameters $(\Delta m^2_i, \sin^2 2\theta_i)$, $i = L, H$, where

$$\begin{aligned} (\Delta m^2_L, \sin^2 2\theta_L) &\cong (\Delta m^2_{\odot}, \sin^2 2\theta_{\odot}) \\ (\Delta m^2_H, \sin^2 2\theta_H) &\cong (\Delta m^2_{atm}, 4|U_{e3}|^2) \quad . \end{aligned} \tag{17}$$

Correspondingly, it can then be described by two points in the $(\Delta m^2, \sin^2 2\theta)$–plane.

The current oscillation data do not determine the mass and flavor spectrum completely. As we have already mentioned in the introduction, the uncertainty is related to:

1. The discrete ambiguity in the solution of the solar neutrino problem: The data favor three solutions indicated in the introduction (SMA, LMA and VO), and some other solutions (*e.g.* the low Δm^2 MSW solution [5, 6], the trimaximal mixing solution [38]), although disfavored, are not excluded. The future solar neutrino experiments will remove this ambiguity and sharpen the determination of the oscillation parameters.

2. The ambiguity in the sign of Δm^2_{32} (and Δm^2_{31}): this determines the type of neutrino mass hierarchy. We refer to the case

$$\Delta m^2_{32} > 0 \quad , \quad i.e. \;\; m_3 > m_2, m_1 \tag{18}$$

as to the spectrum with *normal* mass hierarchy and to the case

$$\Delta m^2_{32} < 0 \quad , \quad i.e. \;\; m_2, m_1 > m_3 \tag{19}$$

as to the spectrum with *inverted* mass hierarchy.

The key difference between these two hierarchies is that, in the normal hierarchy, the small U_{e3}-admixture of ν_e is in the heaviest state whereas in the inverted hierarchy, this admixture is in the lightest state.

The type of hierarchy can in principle be established in future studies of atmospheric neutrinos. If the effects of ν_e oscillations will be observed and the sign of the charged lepton produced by the atmospheric neutrinos will be identified in the future experiments, the studies of matter effects in the neutrino and antineutrino channels will allow to establish the sign of Δm^2. The sign can also be found from the studies of matter effects in the future long baseline experiments, in particular, with neutrino factories.

3. The value of U_{e3} is unknown. In principle, future atmospheric neutrino experiments and the long baseline experiments will be able to measure or further restrict U_{e3}.

4. In the case of the SMA and LMA solutions, $\Delta m^2_{21} > 0$. But the sign of Δm^2_{21} is undetermined in the VO solution. The feasibility of resolving this ambiguity has been recently discussed in [39].

Summarizing, the ambiguity in the present analysis is related to the solution of the solar neutrino problem, the type of hierarchy and the value of U_{e3}. The first two ambiguities lead to six possible schemes of neutrino masses and mixing. Within each scheme, the predictions depend on the value of U_{e3}.

2.3 Neutrino conversion regions

In supernova, the transitions occur mainly in the resonance layers, where the density varies between $(\rho_{res} - \Delta\rho_{res}) \div (\rho_{res} + \Delta\rho_{res})$. Here ρ_{res} is the resonance density:

$$\rho_{res} \approx \frac{1}{2\sqrt{2}G_F}\frac{\Delta m^2}{E}\frac{m_N}{Y_e}\cos 2\theta \quad , \tag{20}$$

G_F is the Fermi constant, m_N is the mass of the nucleon, E is the neutrino energy and Y_e is the electron fraction – the number of electrons per nucleon[5]. For small

[5]It is worthwhile to introduce the resonance density for "VO" parameters too, although the dominating effect could be the vacuum oscillations. We shall consider the limit of $\sin^2 2\theta \to 1$ as a special case.

vacuum mixing, the width of the resonance layer equals

$$2\Delta\rho_{res} \approx 2\rho_{res} \tan 2\theta \quad . \tag{21}$$

Using (20), the resonance matter density can be written as

$$\rho_{res} \sim 1.4 \times 10^6 \text{ g/cc} \left(\frac{\Delta m^2}{1 \text{ eV}^2}\right) \left(\frac{10 \text{ MeV}}{E}\right) \left(\frac{0.5}{Y_e}\right) \cos 2\theta \quad . \tag{22}$$

There are two resonance layers. The layer at higher densities (H-resonance layer), which corresponds to Δm^2_{atm}, is at

$$\rho_H \sim 10^3 - 10^4 \text{ g/cc} \quad , \tag{23}$$

and the layer at lower densities (L-resonance layer), characterised by $\Delta m^2_{\odot}$, is at

$$\rho_L = \begin{cases} 5 - 15 & \text{g/cc} \quad \text{for SMA} \\ 10 - 30 & \text{g/cc} \quad \text{for LMA} \\ < 10^{-4} & \text{g/cc} \quad \text{for VO} \quad . \end{cases} \tag{24}$$

The regions where the neutrino transitions occur are thus far outside the core of the star – in the outer layers of the mantle. Therefore

- the transitions do not influence the dynamics of collapse or the cooling of the core;
- the r-processes, which occur at $\rho \gtrsim 10^5 - 10^6$ g/cc, are also not affected;
- the shock wave does not influence the neutrino conversions (indeed, during the time of cooling by neutrino emission ($t \sim 10$ sec), the shock wave can only reach layers with densities $\rho \gtrsim 10^6$ g/cc [40, 41]);
- the density profile encountered by the neutrinos during their resonant conversions is almost static, and the same as that of the progenitor star.

In the region with densities $\gtrsim 1$ g/cc, the electron fraction is almost constant and the density profile can be approximated by [12, 36, 42]

$$\rho Y_e \approx 2 \cdot 10^4 \text{ g/cc} \left(\frac{r}{10^9 \text{ cm}}\right)^{-3} \quad , \quad \text{for } \rho \gtrsim 1 \text{ g/cc} \; . \tag{25}$$

For $\rho \lesssim 1$ g/cc, the fraction of hydrogen increases and Y_e becomes larger than 0.5. The exact shape of the density profile depends on the details of the composition of the star.

2.4 Factorization of dynamics

The hierarchy of Δm^2, and therefore the hierarchy of the densities of the resonance layers, leads to the "factorization" of dynamics of conversion: the transitions in the two resonance layers can be considered independently and each transition is reduced to a two neutrino problem. Indeed, in the H-resonance region, the mixing U^m_{e2} associated with $\Delta m^2_\odot$ is suppressed by matter. The suppression factor is

$$\frac{U^m_{e2}}{U_{e2}} \sim \frac{\rho_L}{\rho_H} \lesssim 10^{-2} \quad . \tag{26}$$

Correspondingly, the effects driven by $\Delta m^2_\odot$ are suppressed by more than two orders of magnitude.

In the L-resonance region, the mixing associated with Δm^2_{atm} coincides with the vacuum mixing: $U^m_{e3} \approx U_{e3}$. The matter corrections are strongly suppressed:

$$U^m_{e3} = U_{e3}(1 + \mathcal{O}(\xi)) \quad , \qquad \xi \approx \frac{\rho_L}{\rho_H} \lesssim 10^{-2} \quad . \tag{27}$$

That is, the mixing associated with Δm^2_{atm} is almost constant, and therefore the level ν_3 practically does not participate in the dynamics. By an appropriate redefinition of the fields, the problem can be reduced to a two state problem. The state ν_3 decouples from the rest of the system, producing just an averaged oscillation effect [26].

If the mixing U_{e3} is very small, the resulting survival probability of ν_e ($\bar{\nu}_e$) is also factorized [24, 25]:

$$[P(\nu_e \to \nu_e)]_{total} = [P(\nu_e \to \nu_e)]_H \ \times \ [P(\nu_e \to \nu_e)]_L \ + \mathcal{O}(|U_{e3}|^2) \quad , \tag{28}$$

and similarly for $\bar{\nu}_e$.

2.5 Adiabatic, non-adiabatic and transition regions

The dynamics of transitions in each resonance layer is determined by the adiabaticity parameter γ [43, 44]:

$$\gamma \equiv \frac{\Delta m^2}{2E} \frac{\sin^2 2\theta}{\cos 2\theta} \frac{1}{(1/n_e)(dn_e/dr)} \quad , \tag{29}$$

such that the "flip" probability – the probability that a neutrino in one matter eigenstate jumps to the other matter eigenstate – is

$$P_f = exp\left(-\frac{\pi}{2}\gamma\right) \tag{30}$$

as given by the Landau-Zener formula [43]. Adiabatic conversion corresponds to $\gamma \gg 1$, *i.e.* to a very small flip probability [6].

[6] The Landau-Zener formula is valid for a linear variation of density in the resonance region and a small mixing angle θ. For an arbitrary density distribution and mixing angle, the Landau-Zener

Let us consider the density profile of the form

$$\rho = A/r^n \quad , \tag{32}$$

where A is the proportionality constant. From (29), we get the adiabaticity parameter for this profile as

$$\gamma = \frac{1}{2n}\left(\frac{\Delta m^2}{E}\right)^{1-1/n} \frac{\sin^2 2\theta}{(\cos 2\theta)^{1+1/n}} \left(\frac{2\sqrt{2}G_F Y_e}{m_N} A\right)^{1/n} \quad . \tag{33}$$

Here we have used the resonance condition to express r through the oscillation parameters. Note that the dependence of γ on the absolute scale of density, A, is rather weak:

$$\gamma \propto A^{1/n} \quad . \tag{34}$$

For $n = 3$, the change of A by one order of magnitude leads to the change of γ by a factor of 2.

For a fixed density scale A, the value of γ depends on the power index n as

$$\gamma \propto 1/n \quad , \tag{35}$$

so that a variation of n between 2 to 4 leads to the variation in γ by a factor of 2.

In turn, the uncertainty of a factor of 2 in γ is equivalent to the change of $\sin^2 2\theta$ by a factor of 2 (at small values of θ), or the change of Δm^2 by a factor of $2^{n/(n-1)} \sim 3-4$.

The lines of equal γ (and therefore, equal P_f) on the $(\Delta m^2 - \sin^2 2\theta)$ – plot are determined by

$$(\Delta m^2)^{1-1/n} \sin^2 2\theta = const \tag{36}$$

for small θ.

For $n = 3$ which will be used in the further calculations, we get

$$\Delta m^2 = const \,/\, \sin^3 2\theta \quad . \tag{37}$$

From (30) and (33), the flip probability as a function of energy can be written as [27]

$$P_f = \ \mathrm{Exp}\left[-\left(\frac{E_{na}}{E}\right)^{2/3}\right] \quad , \tag{38}$$

where

$$E_{na} = \left(\frac{\pi}{12}\right)^{3/2} \frac{\Delta m^2 \sin^3 2\theta}{\cos^2 2\theta} \left(\frac{2\sqrt{2}G_F Y_e}{m_N} A\right)^{1/2} \quad . \tag{39}$$

The dependence of P_f on E/E_{na} is shown in Fig. 2. One can divide the whole range

formula (30) gets modified to [45]:

$$P_f = \frac{exp(-\frac{\pi}{2}\gamma F) - exp(-\frac{\pi}{2}\gamma F/\sin^2\theta)}{1 - exp(-\frac{\pi}{2}\gamma F/\sin^2\theta)} \quad , \tag{31}$$

where F is a function of the density profile and the mixing angle. The adiabaticity condition is, approximately, $\gamma F \gg 1$. At small mixing angles and linear density variation in the resonance region, $F \approx 1$ and (31) reduces to (30).

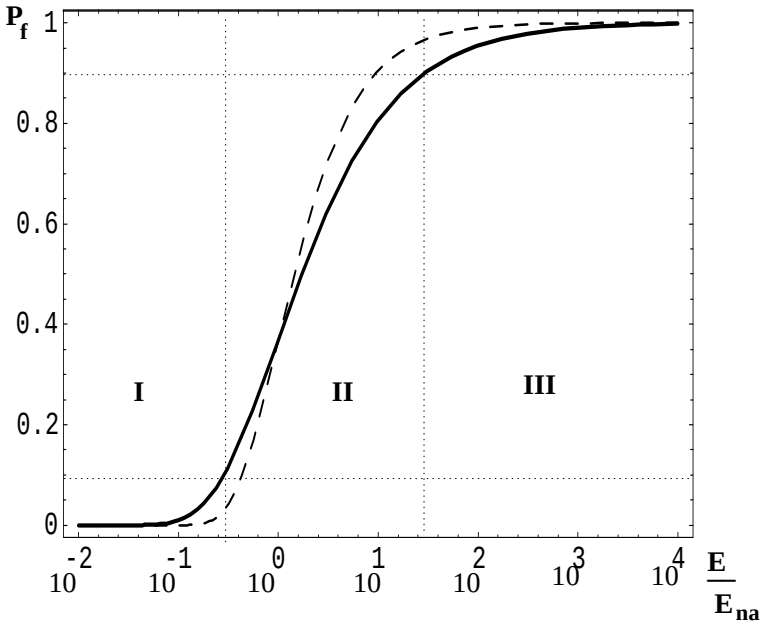

Figure 2: The energy dependence of P_f on E/E_{na}. The solid line is for the density profile $\rho \sim r^{-3}$, whereas the dashed line is for the density profile $\rho \sim e^{-r}$.

of energy in three parts:

For $E/E_{na} < 10^{-1}$ (region I), we get $P_f \approx 0$. In this range, pure adiabatic conversion occurs.

For $E/E_{na} > 10^2$ (region III), the flip probability is close to 1, which corresponds to a strong violation of adiabaticity.

In the transition region $E/E_{na} = 10^{-1} - 10^2$ (region II), P_f increases with the neutrino energy. This region spans almost three orders of magnitude in energy, which is substantially larger than the range of energies in the neutrino spectrum. Notice that for the exponential density distribution (which is the case inside the sun), the transition region is narrower (about two orders of magnitude) and correspondingly, the energy dependence in this region is stronger.

The observable part of the supernova neutrino spectrum lies mainly between the energies of 5 and 50 MeV, *i.e.* it spans about one order of magnitude. If the spectrum is in region I, completely adiabatic conversion occurs for the whole spectrum. In the region II, the conversion depends on energy, however the dependence is not strong over the relevant range of energies. The average energies of any two neutrino species differ by a factor of less than 3, and for $\Delta E/E \sim 3$, the variation in the flip probability is $\Delta P_f \leq 0.2$ (from Fig. 2). In the first approximation, the final spectrum can then be characterized by an *average* or *effective* flip probability. This is illustrated in Fig. 3: the spectra of the number of events taking into account the energy dependence of P_f are shown in (a) and the spectra with an effective flip probability $\langle P_f \rangle$ are shown in (b). It may be observed that the spectra with an appropriate value of $\langle P_f \rangle$ can mimic the features of the actual spectra.

In Fig. 4, we show the contours of equal flip probability P_f (31) in the ($\Delta m^2 -$

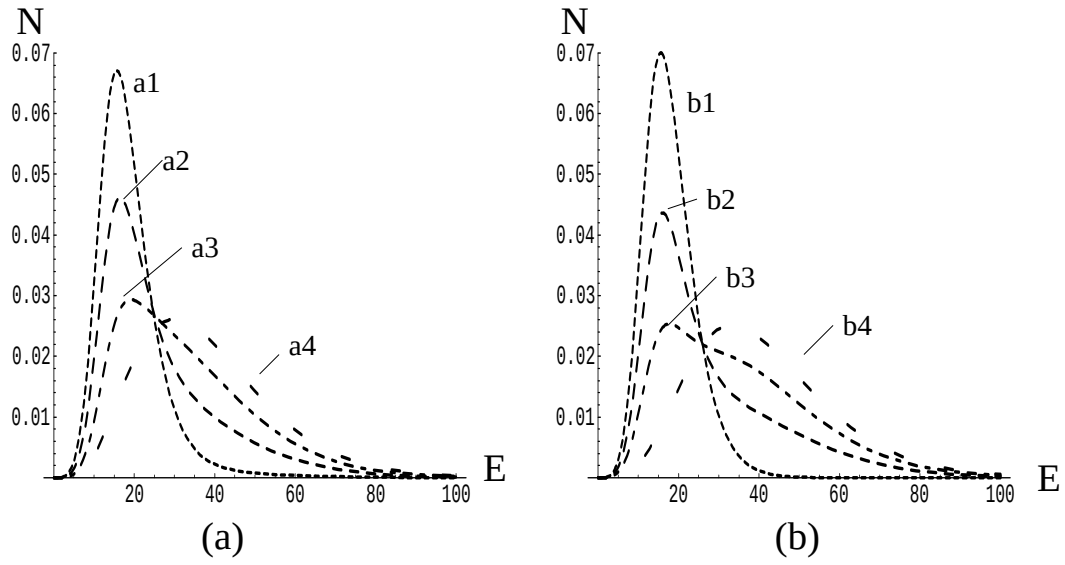

Figure 3: The number of $\nu_e - N$ charged current events, taking into account the energy dependence of the flip probability. The parameters for the original spectra are taken to be $T_e = 3$ MeV, $\eta_e = 3$, $T_x = 8$ MeV, $\eta_x = 1$. In (a), the flip probability is $P_f = Exp[-(E_{na}/E)^{2/3}]$ with (a1): $E_{na} = 0.05$, (a2): $E_{na} = 2$, (a3): $E_{na} = 10$, (a4): $E_{na} = 50$ MeV. In (b), the effective flip probability $\langle P_f \rangle$ is (b1): 1.0, (b2): 0.85, (b3): 0.6, (b4): 0.0

$\sin^2 2\theta$) plot for two different energies on the borders of the observable spectrum. We also show the parameter ranges which explain the solar and atmospheric neutrino data. The dark band (the "atmospheric neutrino band") corresponds to the allowed range of Δm^2_{31}. The rightmost part of this band is excluded by the CHOOZ experiment [4]. The range of $|U_{e3}|^2$ that can be probed by the long baseline experiment MINOS [46] is also shown.

The contours of $P_f = 0.1$ and $P_f = 0.9$ divide the plot into three regions, corresponding to the three regions in fig. 2:

- The "adiabatic region" (I) is the region above the contour with $P_f = 0.1$, where adiabaticity is well satisfied and strong flavor conversions occur.
- The "transition region" (II) is the region between $P_f = 0.1$ and $P_f = 0.9$ contours. Here the adiabaticity is partially broken and the transitions are not complete. Moreover, the extent of transitions depends on the energy.
- The "non-adiabatic" region (III) lies below the $P_f = 0.9$ contour. The neutrino conversions are practically absent.

Since the adiabaticity breaking increases with E and decreases with the increase of Δm^2 and $\sin^2 2\theta$, the lines of equal P_f for $E = 50$ MeV are shifted to larger Δm^2 and $\sin^2 2\theta$ relative to the lines for $E = 5$ MeV. The dependence of the contours of equal P_f on the density profile is rather weak, as can be seen from the previous discussion.

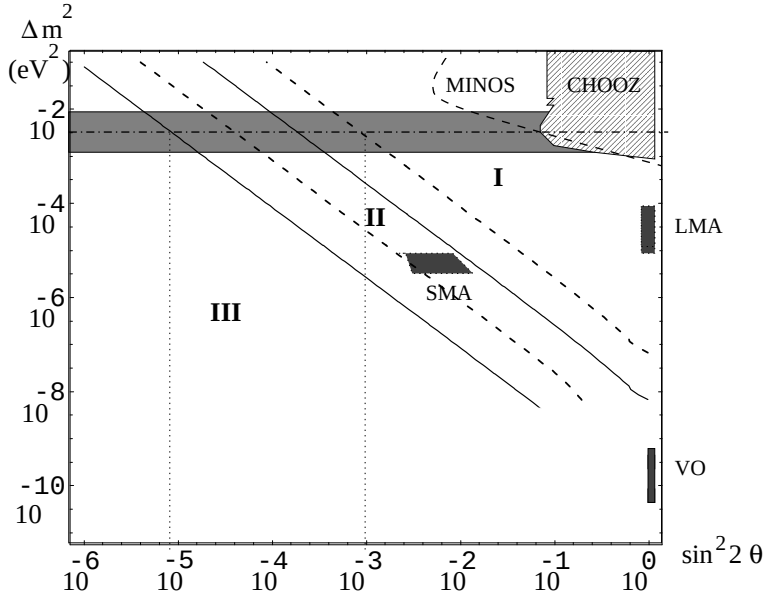

Figure 4: The contours of equal flip probability P_f. The solid lines denote the contours of flip probability for a 5 MeV neutrino: the line on the left stands for $P_f = 0.9$ (highly non-adiabatic transition) and the line on the right stands for $P_f = 0.1$ (adiabatic transition). The dashed lines represent the corresponding flip probabilities for neutrinos with energy 50 MeV. SMA, LMA and VO correspond to the solutions of the solar neutrino anomaly. The two vertical lines indicate the values of $4|U_{e3}|^2 = \sin^2 2\theta$ lying on the borders of the adiabatic, non-adiabatic and transition regions for Δm^2 corresponding to the best fit value of the atmospheric neutrino solution.

Even with conservative estimates, the borders of the regions have an uncertainty of a factor of 2 in $\sin^2 2\theta$ for a given value of Δm^2.

As follows from Fig. 4, the LMA solution lies in the adiabatic region I[7]. The SMA solution is in the transition region. The VO solutions are either in the transition region or in the non-adiabatic region, which depends essentially on the density profile in the outermost layers of the star ($\rho \lesssim 1$ g/cc) and the precise value of Δm^2.

As was described in sect. 2.2, each neutrino mass and flavor spectrum can be represented by two points (17) in the $(\Delta m^2, \sin^2 2\theta)$ plot (Fig. 4). One point, corresponding to $(\Delta m^2_{31}, \sin^2 2\theta_{e3})$, should lie in the atmospheric neutrino band, and the other point corresponding to $(\Delta m^2_{21}, \sin^2 2\theta_{e2})$ should lie in one of the "islands" corresponding to the solutions of the solar neutrino problem. These two points characterize the layers H and L (23,24) respectively. Let $P_H(\bar{P}_H)$ and $P_L(\bar{P}_L)$ be the probabilities that the neutrinos (antineutrinos) jump to another matter eigenstate in these two layers. The extent of conversion is determined by the values of these four flip probabilities.

From Fig. 4, we conclude that the H-resonance is in the adiabatic range (region

[7]The LOW solution also lies in the adiabatic region, so all the results for the LMA scenario are also valid for the LOW scenario.

I) for

$$\sin^2 2\theta_{e3} = 4|U_{e3}|^2 \gtrsim 10^{-3} \quad , \tag{40}$$

and in the transition region (region II) for

$$\sin^2 2\theta_{e3} \sim 10^{-5} - 10^{-3} \quad . \tag{41}$$

As we shall see in sect. 4 and 5, the features of the final spectra depend strongly on the region in which the H resonance lies. According to (41), the supernova neutrino spectra are sensitive to as low values of $4|U_{e3}|^2$ as $10^{-3} - 10^{-5}$. This is more than two orders of magnitude better than the current bounds [4] or those expected from the planned long baseline experiments.

2.6 The level crossing schemes and initial conditions

In the basis of flavor eigenstates $(\nu_e, \nu_\mu, \nu_\tau)$, the evolution of neutrinos at densities $\rho < 10^6$ g/cc relevant for neutrino conversion (see below) is described by a Schrödinger-like equation with the effective Hamiltonian

$$\begin{aligned} H &= \frac{\mathcal{M}^2}{2E} + \mathcal{V} \\ &= \frac{1}{2E} \begin{pmatrix} m^2_{ee} + 2EV & m^2_{e\mu} & m^2_{e\tau} \\ m^2_{e\mu} & m^2_{\mu\mu} & m^2_{\mu\tau} \\ m^2_{e\tau} & m^2_{\mu\tau} & m^2_{\tau\tau} \end{pmatrix} \quad , \end{aligned} \tag{42}$$

where $\mathcal{V} \approx Diag(V, 0, 0)$, and $V = \sqrt{2} G_F n_e$ is the effective potential for the electron neutrinos due to their charged current interactions with electrons.

Since any rotation in the $(\nu_\mu - \nu_\tau)$ subspace does not affect the physics, it is convenient to perform a rotation of the neutrino states $(\nu_e, \nu_\mu, \nu_\tau) \rightarrow (\nu_e, \nu_{\mu'}, \nu_{\tau'})$, which diagonalizes the (ν_μ, ν_τ) submatrix of (42) [47]. (The potential V appears only in the element H_{ee}, and hence is not affected by this rotation.) The effective Hamiltonian in the new basis becomes

$$H = \frac{1}{2E} \begin{pmatrix} m^2_{ee} + 2EV & m^2_{e\mu'} & m^2_{e\tau'} \\ m^2_{e\mu'} & m^2_{\mu'\mu'} & 0 \\ m^2_{e\tau'} & 0 & m^2_{\tau'\tau'} \end{pmatrix} \quad . \tag{43}$$

At $V \gg m^2_{ij}/(2E)$, the off-diagonal terms can be neglected and the Hamiltonian (43) becomes diagonal:

$$H \approx \mathrm{Diag}(V, m^2_{\mu'\mu'}, m^2_{\tau'\tau'}) \quad . \tag{44}$$

That is, the basis states $(\nu_e, \nu_{\mu'}, \nu_{\tau'})$ are the matter eigenstates. These are the states that arrive at the conversion regions as independent (incoherent) states and transform in this region independently.

Notice that a difference between the potentials of ν_μ and ν_τ appears in the second order in the weak interactions due to difference of masses of the μ and τ charged leptons [48]:

$$V_{\mu\tau} \approx V \frac{3 G_F m^2_\tau}{2\sqrt{2}\pi^2 Y_e} \left(\ln \frac{m^2_W}{m^2_\tau} - 1 + \frac{Y_n}{3} \right) \approx 10^{-4}\ V \ , \tag{45}$$

where m_τ is the τ mass, m_W is the W-boson mass, Y_e and Y_n are the numbers of electrons and the neutrons per nucleon respectively. Therefore a complete form of the matrix of potentials is $\mathcal{V} \approx Diag(V, 0, V_{\mu\tau})$.

The potential $V_{\mu\tau}$ becomes important at high densities. One has

$$V_{\mu\tau} \sim \Delta m^2_{atm}/2E \approx 2m^2_{\mu\tau}/2E \text{ at } \rho_{\mu\tau} \sim 10^7 - 10^8 \text{ g/cc}.$$

At $\rho \gg \rho_{\mu\tau}$, and in particular in the region of the neutrinosphere, the potentials V and $V_{\mu\tau}$ dominate over the other terms in the Hamiltonian, and the Hamiltonian becomes approximately diagonal: $H \approx \mathcal{V} \approx \text{Diag}(V, 0, V_{\mu\tau})$. This means that at high densities the flavor states coincide with the eigenstates in medium.

Let us recall that the non-electron neutrinos are produced in the neutral current processes which are flavor blind, *i.e.* they produce a coherent mixture of matter eigenstates. This coherence, however, disappears in the evolution that follows. The ν_e departs from the coherent state due to the large potential V, whereas the coherence of ν_μ and ν_τ is broken by $V_{\mu\tau}$.

In the interval of densities where $V_{\mu\tau} \ll \Delta m^2_{atm}/2E \ll V$, the potential $V_{\mu\tau}$ can be neglected, so that we arrive at the Hamiltonian (43) with eigenstastes $(\nu_e, \nu_{\mu'}, \nu_{\tau'})$. In the region $V_{\mu\tau} \sim \Delta m^2_{atm}/2E$, the level crossing occurs which leads to the transitions $\nu_\mu \to \nu'_\tau$ and $\nu_\tau \to \nu'_\mu$. In the antineutrino channel, we have $\bar\nu_\mu \to \bar\nu'_\mu$ and $\bar\nu_\tau \to \bar\nu'_\tau$.

Since the initial fluxes of ν_μ and ν_τ are equal (F^0_x), we get that the fluxes of $\nu_{\mu'}$ and $\nu_{\tau'}$ will be also equal (F^0_x). Therefore $(\nu_e, \nu_{\mu'}, \nu_{\tau'})$ with fluxes (F^0_e, F^0_x, F^0_x) and correspondingly $(\bar\nu_e, \bar\nu_{\mu'}, \bar\nu_{\tau'})$ with fluxes $(F^0_{\bar e}, F^0_x, F^0_x)$ can be considered as the initial state in our task.

The Hamiltonian (43) allows us easily to construct the level crossing scheme. In Fig. 5, we show the generic level crossing diagrams for the normal and inverted mass hierarchies, for small $\theta_\odot$ (SMA) as well as large $\theta_\odot$ (LMA or VO). The diagonal elements of the Hamiltonian (43), $H_{ii}(n_e)$ $(i = e, \mu', \tau')$, determine the energies of the flavor states shown by the dotted lines. The crossing of these levels indicates a resonance. H and L are the two resonances at higher and lower densities respectively (23,24). The solid lines represent the eigenvalues of the Hamiltonian (43).

In the case of antineutrinos, the effective potential V for the $\bar\nu_e$ has the opposite sign : $V = -\sqrt{2}G_F n_e$. The antineutrinos can then be represented on the same level crossing diagram, as neutrinos travelling through matter with "effectively" negative n_e. The half-plane with positive values of n_e then describes neutrinos and the half-plane with negative values of n_e describes antineutrinos.

The neutrinos (antineutrinos) are produced inside a supernova in regions of high matter density. On their way towards the earth, they travel through a medium with *almost* monotonically decreasing density, towards the vacuum where both neutrinos and antineutrinos have vanishing effective potentials. This corresponds to starting at the right (left) extreme ends of the n_e axis in Fig. 5, and moving towards $n_e = 0$.

The H resonance lies in the neutrino channel for the normal hierarchy and in the antineutrino channel for the inverted hierarchy. The L resonance lies in the neutrino channel for both the hierarchies as long as the solar neutrino solution is SMA or LMA.

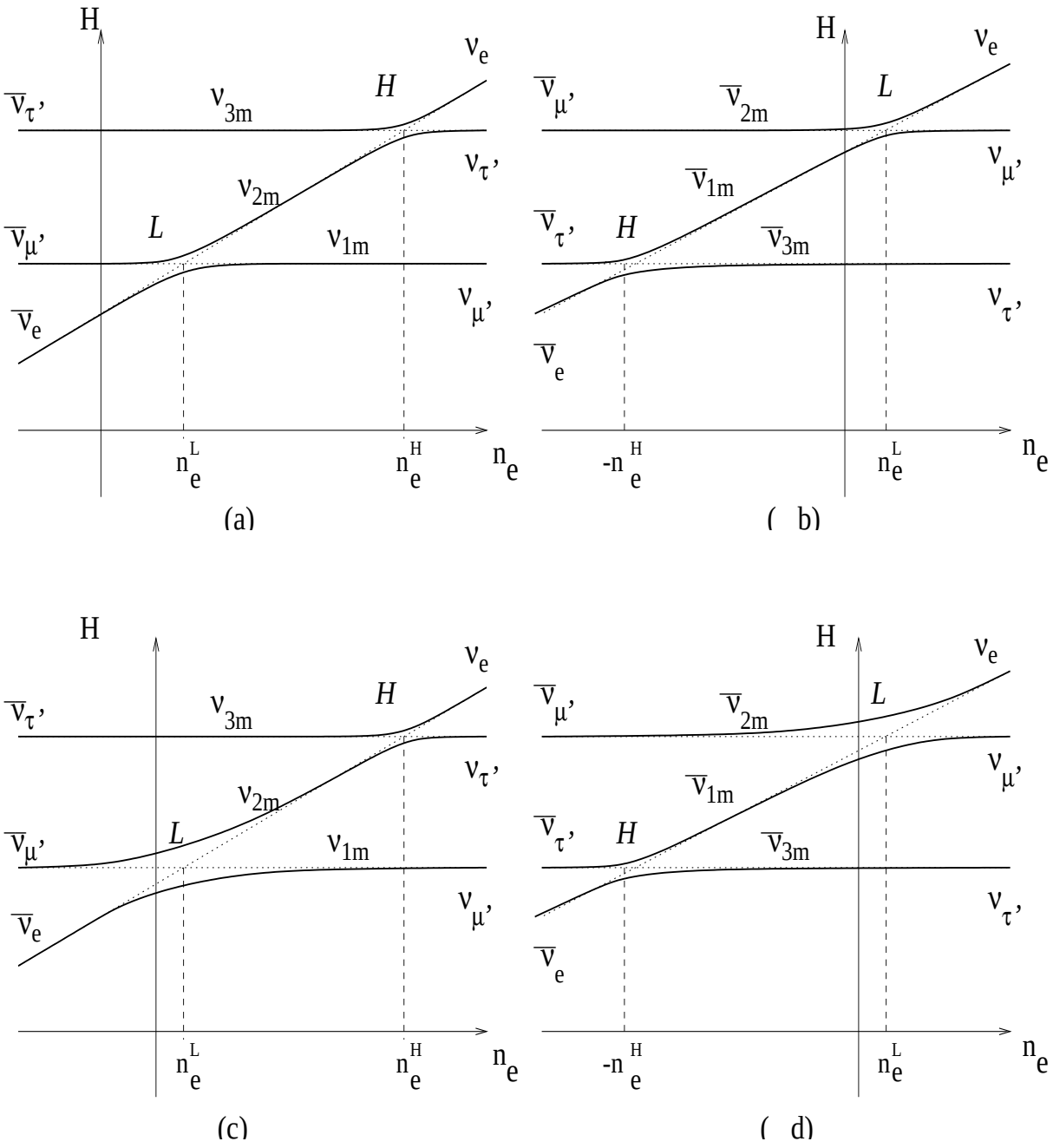

Figure 5: The level crossing diagrams for (a) the normal mass hierarchy and small $\theta_\odot$, (b) the inverted mass hierarchy and small $\theta_\odot$, (c) the normal mass hierarchy and large $\theta_\odot$, (d) the inverted mass hierarchy and large $\theta_\odot$. Solid lines show the eigenvalues of the effective Hamiltonian as functions of the electron number density. The dashed lines correspond to energies of flavor levels ν_e, $\nu_{\mu'}$, and $\nu_{\tau'}$. The part of the plot with $n_e < 0$ corresponds to the antineutrino channel.

For the VO solution, the L resonance may lie in either of the two channels, neutrinos or antineutrinos.

3 Conversion probabilities and the neutrino fluxes at the detectors. The case of normal mass hierarchy

In this section, we derive general expressions for the transition probabilities using the level crossing scheme for the normal mass hierarchy as shown in Figs. 5a and 5c. (The inverted hierarchy will be discussed separately in Sec. 5.)

3.1 Probabilities of conversion inside the star

As has been discussed in sec. 2.6, the neutrino fluxes arise from the central part of the star, in the region of high density. For $\rho \gg \rho_H, \rho_L$, where all the mixings are highly suppressed, the flavor states $(\nu_e, \nu_{\mu'}, \nu_{\tau'})$ coincide with the eigenstates in the medium :

$$\nu_{3m} = \nu_e \quad , \quad \nu_{2m} = \nu_{\tau'} \quad , \quad \nu_{1m} = \nu_{\mu'} \quad . \tag{46}$$

The original fluxes of neutrino eigenstates in the medium equal

$$F^0_{1m} = F^0_x \quad , \quad F^0_{2m} = F^0_x \quad , \quad F^0_{3m} = F^0_e \quad . \tag{47}$$

Let us calculate the fluxes of the mass eigenstates ν_i at the surface of the star. These states, being the eigenstates of the Hamiltonian in vacuum, travel independently to the surface of the earth.

Taking into account that the dynamics of transitions in the two resonance layers are independent (see Sec. 2.4), the fluxes of neutrino mass eigenstates at the surface of the star can be written down directly by tracing the path of the neutrinos in the level crossing diagram. We find the modifications of fluxes in terms of the flip probabilities $P_H, P_L, \bar{P}_H$ and $\bar{P}_L$ introduced in Sec. 2.5.

Let us first calculate the flux of ν_1 at the surface of the star. There are three independent contributions to this flux, from the initial $\nu_e, \nu_{\mu'}$ and $\nu_{\tau'}$ fluxes. The probability that the original state ν_e (which coincides with ν_{3m} in the production region) arrives at the surface of the star as ν_1 is $P_H P_L$, since the state has to flip to the other matter eigenstate at both the resonances. The contribution to the final ν_1 flux from the original ν_e flux is then $P_H P_L F^0_e$. Similarly, the contributions from the original $\nu_{\mu'}$ and $\nu_{\tau'}$ equal $(1 - P_L)F^0_x$ and $P_L(1 - P_H)F^0_x$ respectively. The total ν_1 flux at the surface of the star equals the sum of the three contributions:

$$F_1 = P_H P_L F^0_e + (1 - P_H P_L)F^0_x \quad . \tag{48}$$

Similarly, the fluxes of neutrino mass eigenstates ν_2 and ν_3 arriving at the surface of the star are

$$\begin{aligned} F_2 &= (P_H - P_H P_L)F^0_e + (1 - P_H + P_H P_L)F^0_x \quad , \\ F_3 &= (1 - P_H)F^0_e + P_H F^0_x \quad . \end{aligned} \tag{49}$$

Due to the divergence of the wavepackets, any coherence between the mass eigenstates is lost on the way to the earth. Indeed, over a distance L, the two wavepackets corresponding to two mass eigenstates with a given Δm^2 and having an energy E separate from each other by a distance

$$\Delta L = \frac{\Delta m^2}{2E^2}\ L \quad . \tag{50}$$

Even for the smallest $\Delta m^2 \sim 10^{-10}$ eV^2, for $E \sim 10$ MeV and $L \sim 10$ kpc $\sim 10^{22}$ cm, we get $\Delta L \sim 10^{-2}$ cm. The lengths of the individual wavepackets are $\sigma \lesssim 1/T \sim 10^{-11}$ cm (where T is the temperarture of the production region) is much smaller.

The spread of the wavepackets implies that the neutrinos arrive at the surface of the earth as incoherent fluxes of the mass eigenstates. Upto a geometrical factor of $1/L^2$, they coincide with the fluxes given in (48,49). We can rewrite them as

$$F_i = a_i F_e^0 + (1 - a_i) F_x^0 \quad , \tag{51}$$

with

$$a_1 = P_H P_L,\ a_2 = P_H(1 - P_L),\ a_3 = 1 - P_H \quad . \tag{52}$$

The factor of $1/L^2$ is implicit in the fluxes at the earth.

Using (51), we find the net flux of electron neutrinos at the earth:

$$\begin{aligned} F_e &= \sum_i |U_{ei}|^2 F_i \\ &= F_e^0 \sum_i |U_{ei}|^2 a_i + F_x^0 (1 - \sum_i |U_{ei}|^2 a_i) \quad , \end{aligned} \tag{53}$$

where we have taken into account the unitarity condition $\sum |U_{ei}|^2 = 1$. The final electron neutrino flux reaching the earth can thus be written as

$$F_e = p F_e^0 + (1 - p) F_x^0 \quad , \tag{54}$$

where

$$\begin{aligned} p &\equiv \sum_i |U_{ei}|^2 a_i \\ &= |U_{e1}|^2 P_H P_L + |U_{e2}|^2 (P_H - P_H P_L) + |U_{e3}|^2 (1 - P_H) \quad . \end{aligned} \tag{55}$$

According to (54), p may be interpreted as the total survival probability of electron neutrinos.

The original total flux of the neutrinos ν_e, ν_μ, ν_τ is $F_e^0 + 2F_x^0$. Using the conservation of flux, we find the combined flux of ν_μ and ν_τ at the earth $(F_\mu + F_\tau)$ as

$$F_\mu + F_\tau = (1 - p) F_e^0 + (1 + p) F_x^0 \quad . \tag{56}$$

Note that the final fluxes of the flavor states at the earth (54,56) can be written in terms of only the survival probability p. This is a consequence of two facts: 1) at each transition, one of the neutrinos is decoupled so that the task reduces to 2ν mixing, and 2) the original fluxes of $\nu_{\mu'}$ and $\nu_{\tau'}$ are equal.

3.2 Conversion probabilities for antineutrinos

Let us consider the antineutrino transitions. In the high matter density region ($\rho \gg \rho_H, \rho_L$), the antineutrino flavor eigenstates coincide with the eigenstates in the medium as (see Figs. 5a, 5c):

$$\bar{\nu}_{1m} = \bar{\nu}_e \ , \ \bar{\nu}_{2m} = \bar{\nu}_{\mu'} \ , \ \bar{\nu}_{3m} = \bar{\nu}_{\tau'} \ \ , \tag{57}$$

so that the original fluxes of antineutrino eigenstates in the medium equal

$$\bar{F}^0_{1m} = F^0_{\bar{e}} \ \ , \ \ \bar{F}^0_{2m} = F^0_x \ \ , \ \ \bar{F}^0_{3m} = F^0_x \ \ . \tag{58}$$

The small mixing angle θ_{e3} is further suppressed in the medium, so the $\bar{\nu}_e \leftrightarrow \bar{\nu}_3$ transitions are negligible. The state $\bar{\nu}_{3m}$, being far from the level crossings, propagates adiabatically: $\bar{\nu}_{\tau'} \to \bar{\nu}_3$. Depending on the parameters of the solution for the solar neutrino problem, the propagation of the other two states may be adiabatic or non-adiabatic [19]. From considerations similar to those in the neutrino channel, we get

$$F_{\bar{e}} = \bar{p} F^0_{\bar{e}} + (1 - \bar{p}) F^0_x \ \ , \tag{59}$$

where $\bar{p}$, the survival probability of $\bar{\nu}_e$, equals

$$\bar{p} = |U_{e1}|^2 (1 - \bar{P}_L) + |U_{e2}|^2 \bar{P}_L \ \ . \tag{60}$$

In the case of completely adiabatic propagation, $\bar{P}_L = 0$ and

$$\bar{p} = |U_{e1}|^2 . \tag{61}$$

Let $F_{\bar{\mu}} + F_{\bar{\tau}}$ be the combined flux of $\bar{\nu}_\mu$ and $\bar{\nu}_\tau$. From (59) and the conservation of flux, we get the combined flux of non-electron antineutrinos:

$$F_{\bar{\mu}} + F_{\bar{\tau}} = (1 - \bar{p}) F^0_{\bar{e}} + (1 + \bar{p}) F^0_x \ \ . \tag{62}$$

From (56) and (62), the total flux of the non-electron neutrinos (including antineutrinos) is

$$\begin{aligned} 4F_x &= F_\mu + F_\tau + F_{\bar{\mu}} + F_{\bar{\tau}} \\ &= (1 - p) F^0_e + (2 + p + \bar{p}) F^0_x + (1 - \bar{p}) F^0_{\bar{e}} \ \ . \end{aligned} \tag{63}$$

Summarizing, the equations (54,59, 63) can be written in the compact notation

$$\begin{pmatrix} F_e \\ F_{\bar{e}} \\ 4F_x \end{pmatrix} = \begin{pmatrix} p & 0 & 1-p \\ 0 & \bar{p} & 1-\bar{p} \\ 1-p & 1-\bar{p} & 2+p+\bar{p} \end{pmatrix} \begin{pmatrix} F^0_e \\ F^0_{\bar{e}} \\ F^0_x \end{pmatrix} \ \ . \tag{64}$$

The above general expression holds for both, the normal and the inverted mass hierarchy. The survival probabilities p and $\bar{p}$ for the normal hierarchy are given in (55) and (60) respectively. These probabilities depend on the specific parameters of the masses and mixing scheme.

3.3 Earth matter effects on the ν_e spectrum

The neutrino trajectory inside the earth before reaching the detector depends on the direction of the supernova relative to the earth and the time of the day. The comparison of signals from different detectors would allows one to reveal the earth matter effects. Also certain features of the energy spectra can reveal the earth matter effect even from the observations in one detector.

The mass eigenstates arriving at the surface of the earth oscillate in the earth matter. Let P_{ie} be the probability that a mass eigenstate ν_i entering the earth reaches the detector as a ν_e. The flux of ν_e at the detector is

$$F_e^D = \sum_i P_{ie} F_i \quad . \tag{65}$$

Inserting F_i from (51), we get

$$F_e^D = F_e^0 \sum a_i P_{ie} + F_x^0 (1 - \sum_i a_i P_{ie}) \quad , \tag{66}$$

where a_i's are as defined in (52), and we have used the unitarity condition $\sum_i P_{ie} = 1$. Thus, the ν_e flux at the detector can be written as

$$F_e^D = p^D F_e^0 + (1 - p^D) F_x^0 \quad , \tag{67}$$

with

$$p^D = \sum_i a_i P_{ie} \quad . \tag{68}$$

Comparing F_e^D (67) with F_e (54), we find the difference in the ν_e fluxes at the detector due to the propagation in earth equals

$$F_e^D - F_e = (p^D - p)(F_e^0 - F_x^0) \quad , \tag{69}$$

where p is given in (55). The earth matter effect can be quantified by the difference of probabililty $(p^D - p)$:

$$p^D - p = \sum_i a_i (P_{ie} - |U_{ei}|^2) \quad . \tag{70}$$

Using definitions in (52) and $\sum_i P_{ie} = 1$, we can write explicitly

$$p^D - p = P_H (P_{2e} - |U_{e2}|^2)(1 - 2P_L) + (P_{3e} - |U_{e3}|^2)(1 - P_H - P_H P_L) \quad . \tag{71}$$

The second term in (71) can be neglected. Indeed, inside the earth, ν_3 oscillates with a very small depth:

$$P_{3e} - |U_{e3}|^2 \lesssim \left(\frac{2EV_{earth}}{\Delta m^2_{atm}} \right) \sin^2 2\theta_{e3} \quad , \tag{72}$$

where V_{earth} is the effective potential of ν_e in the earth. For neutrino energies of 5 – 50 MeV, we have $2EV_{earth}/\Delta m^2_{atm} \lesssim 10^{-2}$. Moreover, $\sin^2 2\theta_{e3} \leq 0.1$, so that

$$P_{3e} - |U_{e3}|^2 \leq 10^{-3} \quad . \tag{73}$$

Finally, we can write

$$p^D - p \approx P_H(P_{2e} - |U_{e2}|^2)(1 - 2P_L) \quad . \tag{74}$$

In general, when the signals from two detectors D1 and D2 are compared, we get the difference of fluxes

$$F_e^{D1} - F_e^{D2} \approx P_H \cdot (1 - 2P_L) \cdot (P_{2e}^{(1)} - P_{2e}^{(2)}) \cdot (F_e^0 - F_x^0) \quad . \tag{75}$$

where $P_{2e}^{(1)}$ and $P_{2e}^{(2)}$ are the $\nu_e \leftrightarrow \nu_2$ oscillation probabilities for the detectors D1 and D2 correspondingly.

According to (75) the earth matter effect is factorized: it is proportional to the difference in the original ν_e and ν_x fluxes, the conversion factor $P_H(1 - 2P_L)$ inside the star, and the difference of earth oscillation probabilities P_{2e} at the two detectors. Let us consider these factors separately.

1) $F_e^0 - F_x^0$: Since the ν_e spectrum is softer than the ν_x spectrum, and the luminosities of both the spectra are similar in magnitude [49], the term $(F_e^0 - F_x^0)$ is positive at low energies and becomes negative at higher energies where the ν_x flux overwhelms the ν_e flux. Therefore, the earth effect has a different sign for low and high energies, and there exists a critical energy E_c, such that $F_e^0(E_c) = F_x^0(E_c)$, where this change of sign takes place. Since the cross section of the neutrino interactions increases with energy, the Earth effect is expected to be more significant at higher energies (if all the other factors are only weakly sensitive to the neutrino energy).

2) $P_H(1-2P_L)$: This factor characterizes the neutrino conversions inside the star. P_H can be looked upon as a suppression factor due to the conversions at the higher resonance. Indeed, in the limit of $U_{e3} \to 0$ and $P_H \to 1$, (74) reduces to the expression for the earth effects in the case of two neutrino mixing :

$$[p^D - p]_{2\nu} = (P_{2e} - |U_{e2}|^2)(1 - 2P_L) \tag{76}$$

which is equivalent to the one used in literature [50] in the context of day-night effect for solar neutrinos. Therefore (74) can be looked upon as the earth matter effect due to the two neutrino mixing (76) suppressed by a factor of P_H. The mixing of the third neutrino thus plays a major role, making the expected earth effects in the case of supernova neutrinos smaller than those expected in the case of solar neutrinos for the same mixing scheme and in the same energy range. If the H-resonance is completely adiabatic, the earth effect vanishes: all the ν_e produced are converted to ν_3 in the star, and the earth matter effect on ν_3 is negligibly small (as we have established through (72)).

3) $P_{2e}^{(1)} - P_{2e}^{(2)}$: If the neutrino trajectory crosses only the mantle of the earth, one can use a constant density approximation which gives

$$P_{2e}^{(1)} - P_{2e}^{(2)} \approx \sin 2\theta_{e2}^m \ \sin(2\theta_{e2}^m - 2\theta_{e2}) \ \left[\sin^2\left(\frac{\pi d_1}{l_m}\right) - \sin^2\left(\frac{\pi d_2}{l_m}\right)\right] \quad . \tag{77}$$

Here θ_{e2}^m and l_m are the mixing angle and oscillation length inside the earth respectively, and d_i is the distance travelled by the neutrinos inside the earth before reaching

the detector D_i. The first two terms on the right hand side of (77) are positive for the scenarios with the SMA and LMA solutions, so that the sign of $(P_{2e}^{(1)} - P_{2e}^{(2)})$ is the same as the sign of the term inside the square bracket in (77). For the scenario with the VO solution, the earth matter effects are negligible: for $\Delta m^2 \sim 10^{-10}$ eV^2, the mixing in the earth matter is highly suppressed, so that $\sin 2\theta_{e2}^m$ in (77) is very small.

If neutrinos cross both the mantle and the core, the parametric enhancement of oscillations may occur, which leads to the appearance of parametric peaks apart from the peaks due to the MSW resonances in the core and the mantle [51]. Correspondingly the factor $(P_{2e}^{(1)} - P_{2e}^{(2)})$ will be a more complicated function of the neutrino energy.

To summarize, the earth matter effects on the ν_e spectrum can be significant only for the scenarios with the SMA or LMA or LOW solutions. Moreover, the H resonance needs to be non-adiabatic in the case of normal mass hierarchy.

3.4 Earth matter effects on the $\bar{\nu}_e$ spectrum

The oscillation effects, are determined by the survival probability of the electron antineutrinos, $\bar{p}^D$, at the detector. Considerations similar to those for (60) lead to

$$\bar{p}^D = \bar{P}_{1e}(1 - \bar{P}_L) + \bar{P}_{2e}\bar{P}_L \quad . \tag{78}$$

Then from Eqs. (59), (60) and (78), we obtain

$$F_{\bar{e}}^D - F_{\bar{e}} = (\bar{P}_{1e} - |U_{e1}|^2) \cdot (1 - 2\bar{P}_L) \cdot (F_{\bar{e}}^0 - F_x^0) \quad , \tag{79}$$

where we have neglected the oscillations of $\bar{\nu}_3$ inside the earth. Generalizing the result in (79), we find the difference in the fluxes at two detectors $D1$ and $D2$:

$$F_{\bar{e}}^{D1} - F_{\bar{e}}^{D2} \approx (\bar{P}_{1e}^{(1)} - \bar{P}_{1e}^{(2)}) \cdot (1 - 2\bar{P}_L) \cdot (F_{\bar{e}}^0 - F_x^0) \quad . \tag{80}$$

The earth matter effects for the antineutrinos are thus also factorized: they are proportional to the difference in the original ν_e and ν_x fluxes, the factor of $(1 - 2\bar{P}_L)$ which depends on the conversions inside the star, and the difference $(\bar{P}_{1e}^{(1)} - \bar{P}_{1e}^{(2)})$ between the oscillation probabilities inside the Earth for the neutrinos reaching the two detectors. Note that due to the absence of the H-resonance in the antineutrino channel, there is no suppression factor similar to P_H (75) in the neutrino case.

The factor $(F_{\bar{e}}^0 - F_x^0)$ is positive at low energies and negative at high energies. The matter effects then change sign at an energy $\bar{E}_c$ where $F_{\bar{e}}^0(\bar{E}_c) = F_x^0(\bar{E}_c)$. Since the neutrino cross section increases with energy, the observed effect is expected to be larger at higher energies (if all the other factors are only weakly sensitive to the antineutrino energy).

In the approximation of a constant density, the factor depending on the oscillation probabilities inside the earth is

$$\bar{P}_{1e}^{(1)} - \bar{P}_{1e}^{(2)} \approx -\sin 2\bar{\theta}_{e2}^m \ \sin(2\bar{\theta}_{e2}^m - 2\theta_{e2}) \ \left[\sin^2\left(\frac{\pi d_1}{l_m}\right) - \sin^2\left(\frac{\pi d_2}{l_m}\right)\right] \quad , \tag{81}$$

where $\bar{\theta}^m_{e2}$ is the mixing angle inside the earth for the antineutrinos. For the antineutrino channel $\bar{\theta}^m_{e2} < \theta_{e2} \ll 1$ for SMA solution and $\bar{\theta}^m_{e2}$ is strongly suppressed by matter in the VO case. Therefore the earth matter effects on the $\bar{\nu}_e$ spectrum can be significant only for the scenario with the LMA (as well as LOW) solution. In this scenario, $\sin 2\bar{\theta}^m_{e2} > 0$ and $\sin(2\bar{\theta}^m_{e2} - 2\theta_{e2}) < 0$, so that according to (81), the sign of $(\bar{P}^{(1)}_{1e} - \bar{P}^{(2)}_{1e})$ is the same as the sign of the oscillation term inside the square bracket in (81).

To summarize, in the case of normal mass hierarchy, the earth matter effects on the $\bar{\nu}_e$ spectrum are significant only for the scenario with the LMA solution. The effects are practically unaffected by the mixing of $\bar{\nu}_3$ and change sign at an energy $\bar{E}_c$ such that $F^0_{\bar{e}}(\bar{E}_c) = F^0_x(\bar{E}_c)$.

4 Effects of neutrino conversion for the mass spectra with normal hierarchy

In this section, we shall consider the neutrino conversion effects for specific 3ν schemes with the normal mass hierarchy. The general expressions for the transition probabilities and the neutrino fluxes at the detectors are given in Sec. 3, where they are expressed in terms of the total survival probabilities p and $\bar{p}$ of electron neutrinos and electron antineutrinos respectively. The values of p and $\bar{p}$ need to be calculated separately for each specific scheme. Notice that, given a scheme, the least known parameter is $|U_{e3}|^2$. We shall consider the effects of neutrino conversion in the three possible regions of $|U_{e3}|^2$: these correspond to the regions I, II and III as described in Sec. 2 (see also Figs. 2 and 3.)

4.1 The scheme with the SMA solution

The mass and flavor spectrum of the scheme is shown in Fig. 6. The non-electron neutrinos ν_μ and ν_τ mix strongly in the mass eigenstates ν_2 and ν_3. The electron flavor is weakly mixed: it is mainly in ν_1 with small admixtures in the heavy states. The solar neutrino data is explained via the small mixing angle MSW solution, with the parameters as given in (3). The level crossing scheme is shown in Fig. 5a. Both the resonances are in the neutrino channel.

In this scheme,

$$|U_{e1}|^2 \approx 1 \quad , \quad |U_{e2}|^2 \approx \frac{1}{4}\sin^2 2\theta_\odot \sim 10^{-3} \quad . \tag{82}$$

Let us first consider the antineutrino channels. There is no resonance here, and the mixing in matter is suppressed. As a consequence, the adiabaticity condition is fulfilled in the L layer and $\bar{P}_L \approx 0$. Then according to the level crossing scheme (Fig. 5a), the following transitions occur inside the star:

$$\bar{\nu}_e \to \bar{\nu}_1 \quad , \quad \bar{\nu}_{\mu'} \to \bar{\nu}_2 \quad , \quad \bar{\nu}_{\tau'} \to \bar{\nu}_3 \quad .$$

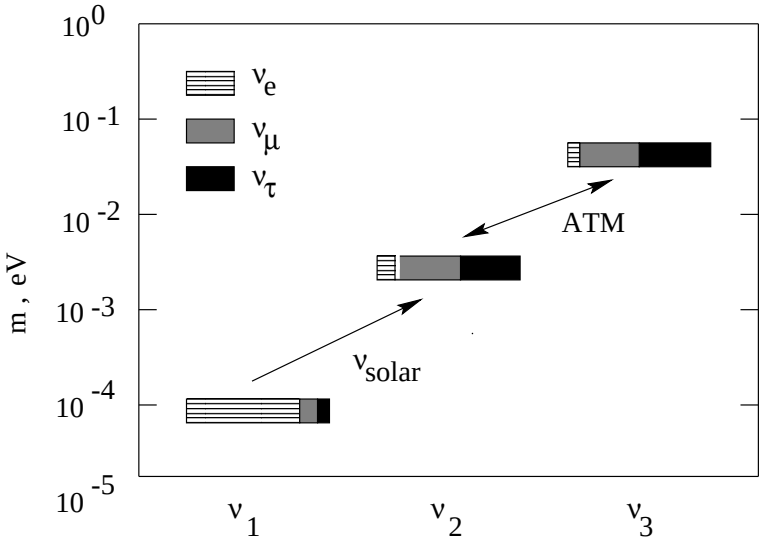

Figure 6: Neutrino mass and mixing pattern for the scheme with the small mixing angle MSW solution of the solar neutrino problem. The boxes correspond to the mass eigenstates. The sizes of different regions in the boxes show admixtures of different flavors. Weakly hatched regions correspond to the electron flavor, strongly hatched regions depict the muon flavor, black regions represent the tau flavor.

Using $|U_{e2}|^2 \ll 1$ and $\bar{P}_L \approx 0$, we get from (60) the survival probability for $\bar{\nu}_e$:

$$\bar{p} \approx |U_{e1}|^2(1 - \bar{P}_L) \approx 1 \quad . \tag{83}$$

Let us consider now neutrino channels. The value of the ν_e survival probability p depends on the region in which the oscillation parameters of the H resonance lie.

Region I: Since the H resonance is adiabatic, the level crossing scheme (Fig. 5a) leads to the following transitions:

$$\nu_e \to \nu_3 \quad , \quad \nu_{\mu'} \to \nu_1, \nu_2 \quad , \quad \nu_{\tau'} \to \nu_1, \nu_2 \quad .$$

At $P_H \approx 0$, the Eq. (55) gives

$$p \approx |U_{e3}|^2 \leq 0.03 \quad . \tag{84}$$

The flavor transitions are then complete, and independent of the adiabaticity at the L resonance.

The final neutrino (and antineutrino) fluxes are

$$F_e \approx F_x^0 \quad , \quad F_{\bar{e}} \approx F_{\bar{e}}^0 \quad , \quad 4F_x \approx F_e^0 + 3F_x^0 \quad . \tag{85}$$

The neutrino spectra have the following features:

- The neutronization ν_e peak disappears (it is suppressed by a factor of $|U_{e3}|^2 \leq 0.03$). Instead one would expect a ν_x neutronization peak which may be detected by the neutral current interactions.

- The antineutrino signal is practically unchanged.
- The ν_e has the hard spectrum of F_x^0, and therefore

$$\langle E_{\nu_e} \rangle > \langle E_{\bar{\nu}_e} \rangle \quad ,$$

  which is a clear signal of mixing.
- The ν_x spectrum is *composite, i.e.* it contains both the soft (original ν_e) and the hard (original ν_x) components.

The earth matter effects on the ν_e spectrum (75) are suppressed by the factor of $P_H \approx 0$. Also, since the mixing in the antineutrino channel is suppressed in matter, the earth matter effects on the $\bar{\nu}_e$ spectrum are negligible. As a result, one expects practically the same neutrino (and antineutrino) signal in all detectors.

Region II. Neutrinos jump partially between the third and the second levels in H region, so that the following transitions occur:

$$\nu_e \rightarrow \nu_1, \nu_2, \nu_3 \quad , \quad \nu_{\mu'} \rightarrow \nu_1, \nu_2 \quad , \quad \nu_{\tau'} \rightarrow \nu_1, \nu_2, \nu_3 \quad .$$

The ν_e survival probability p is given by the general formula (55). The value of P_H, and hence the survival probability p, depends on the neutrino energy, although this dependence is relatively weak, as demonstrated in Figs. 2 and 3.

The features of the spectra are:

- the neutronization peak is distributed in both, ν_e and ν_x,
- the ν_e and ν_x spectra are composite,
- the $\bar{\nu}_e$ spectrum is unchanged.

The earth matter effects can be observed in the ν_e spectrum. The magnitude of the effects is proportional to P_H (75). For $\bar{\nu}_e$ spectrum the effect is negligible.

Region III. No conversion occurs at the H resonance, so that in the star

$$\nu_e \rightarrow \nu_1, \nu_2 \quad , \quad \nu_{\mu'} \rightarrow \nu_1, \nu_2 \quad , \quad \nu_{\tau'} \rightarrow \nu_3 \quad .$$

From (55) and (82) we get using $P_H \approx 1$:

$$p \approx |U_{e1}|^2 P_L + |U_{e2}|^2 (1 - P_L) \approx P_L \quad . \tag{86}$$

The features of the spectra are the same as those described above in the case of region II.

The earth matter effects on the ν_e spectrum in the SMA scheme can be significant in regions II and III, where the factor of P_H is of the order of unity. Indeed, in (77), the value of $(P_{2e} - |U_{e2}|^2)$ can be as large as 0.25 in the energy range of 20-40 MeV, where the term $(F_e^0 - F_x^0)$ is also significant.

In Fig. 7, we show the ν_e spectrum for different distances travelled by the neutrinos through the earth. As follows from Fig. 7, the net effect is $\lesssim 10\%$ even with optimistic values of P_H, P_L and θ_{e2}.

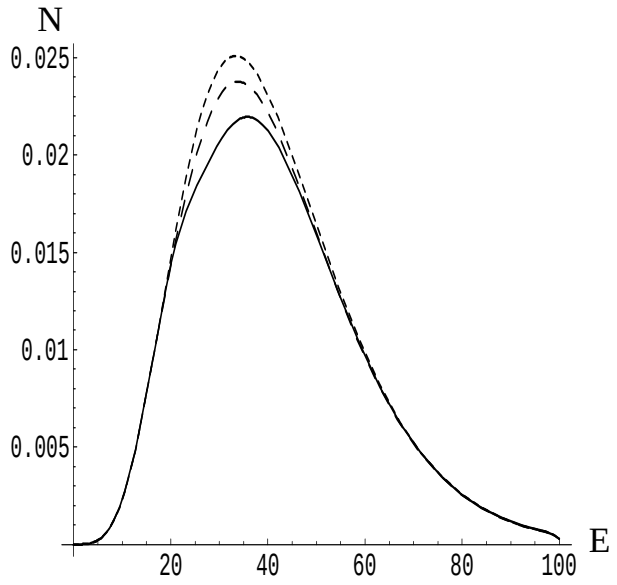

Figure 7: The earth matter effects on the ν_e spectrum for $P_H = 1$ and $P_L = 0$ in the scheme with the SMA solution ($\Delta m^2 = 10^{-5}$ eV^2 , $\sin^2 2\theta_\odot = 10^{-2}$). The dotted, dashed and solid lines show the number of $\nu_e - N$ charged current events when the distance travelled by the neutrinos through the mantle of the earth is $d = 0$ km, $d = 6000$ km, and $d = 10000$ km respectively.

4.2 The scheme with the LMA solution

The mass and flavor spectrum of the scheme is shown in Fig. 8. The solar neutrino data is explained via the $\nu_e \to \nu_2$ resonant conversion inside the sun with a large vacuum mixing angle (4). The level crossing scheme is shown in Fig. 5c. It differs from the previous one by the mixing at the L-resonance. Since the vacuum mixing angle $\theta_\odot$ is large, there is a significant $\bar{\nu}_e \leftrightarrow \bar{\nu}_2$ conversion even though the antineutrinos do not encounter any resonances. The evolution is adiabatic in the antineutrino channel in both the H and L layers. The following transitions occur:

$$\bar{\nu}_e \to \bar{\nu}_1 \quad , \quad \bar{\nu}_{\mu'} \to \bar{\nu}_2 \quad , \quad \bar{\nu}_{\tau'} \to \bar{\nu}_3 \quad .$$

Using $\bar{P}_L \approx 0$, the $\bar{\nu}_e$ survival probability (60) equals

$$\bar{p} \approx |U_{e1}|^2 \approx \cos^2\theta_\odot \quad . \tag{87}$$

Let us consider transitions in the neutrino channels. The L-resonance is adiabatic (Fig. 4), $P_L \approx 0$, and from (55), we get the ν_e- survival probability

$$\begin{aligned} p &\approx |U_{e2}|^2 P_H + |U_{e3}|^2 (1 - P_H) \\ &\approx \sin^2\theta_\odot P_H + |U_{e3}|^2 (1 - P_H) \quad . \end{aligned} \tag{88}$$

Notice that, depending on the value of P_H, the ν_e- survival probability takes the values between

$$|U_{e3}|^2 \leq p \leq |U_{e2}|^2 \quad . \tag{89}$$

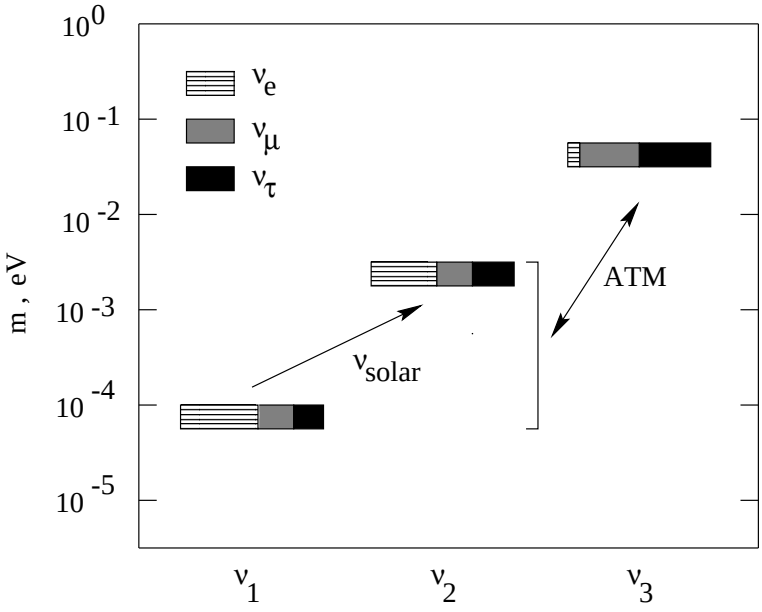

Figure 8: Neutrino mass and mixing pattern of the scheme with the large mixing angle MSW solution for the solar neutrino problem.

The fluxes at the earth are determined by (64), with p and $\bar{p}$ given in (88) and (87). Their features depend on the adiabaticity at the H resonance, which is decided by the region in which $|U_{e3}|^2$ lies.

Region I. The level crossing scheme (Fig. 5c) with adiabatic transitions in the H resonance layer leads to the following transitions inside the star:

$$\nu_e \to \nu_3 \quad , \quad \nu_{\mu'} \to \nu_1 \quad , \quad \nu_{\tau'} \to \nu_2 \quad .$$

Since $P_H \approx 0$ we get $p \approx |U_{e3}|^2$, and the final spectra at the earth:

$$\begin{aligned} F_e &\approx |U_{e3}|^2 F_e^0 + (1 - |U_{e3}|^2) F_x^0 \approx F_x^0 \quad , \\ F_{\bar{e}} &\approx \cos^2\theta_\odot F_{\bar{e}}^0 + \sin^2\theta_\odot F_x^0 \quad , \\ 4F_x &\approx F_e^0 + \sin^2\theta_\odot F_{\bar{e}}^0 + (2 + \cos^2\theta_\odot) F_x^0 \quad . \end{aligned} \tag{90}$$

The following features can be observed:

- The neutronization peak almost disappears from the ν_e channel (suppressed by a factor of $|U_{e3}|^2 \lesssim 0.03$) and appears in the ν_x channel.
- The $\bar{\nu}_e$ spectrum is composite: A mixture of the original $\bar{\nu}_e$ spectrum and the original harder ν_x spectrum, is determined by the solar neutrino mixing angle. This feature distinguishes the LMA scheme from the one with the SMA solution.
- The ν_e spectrum is hard, practically coinciding with the original ν_x spectrum. This leads to

$$\langle E_{\nu_e} \rangle > \langle E_{\bar{\nu}_e} \rangle \quad .$$

- The ν_x spectrum contains components of all the three original spectra $(\nu_e, \bar{\nu}_e, \nu_x)$.

No earth matter effects are expected in the ν_e spectrum, since $P_H \approx 0$. At the same time, the $\bar{\nu}_e$ spectrum can show significant earth matter effects. This is an important signature of the scenario.

Region II. The jump probability in H resonance is substantial and the following transitions occur:

$$\nu_e \to \nu_2, \nu_3 \quad , \quad \nu_{\mu'} \to \nu_1 \quad , \quad \nu_{\tau'} \to \nu_2, \nu_3 \quad .$$

The final spectra are determined by (64) with p given by (88):

$$p \approx \sin^2\theta_\odot \; P_H \quad .$$

Depending on P_H and $\sin^2\theta_\odot \approx |U_{e2}|^2 \approx 0.2 - 0.4$, the probability p can take values between 0.02 and 0.4.

The final spectra can be written as

$$\begin{aligned} F_e &\approx \sin^2\theta_\odot P_H F_e^0 + (1 - \sin^2\theta_\odot P_H) F_x^0 \\ F_{\bar{e}} &\approx \cos^2\theta_\odot F_{\bar{e}}^0 + \sin^2\theta_\odot F_x^0 \\ 4F_x &\approx (1 - \sin^2\theta_\odot P_H) F_e^0 + \sin^2\theta_\odot F_{\bar{e}}^0 + (3 - \sin^2\theta_\odot + \sin^2\theta_\odot P_H) F_x^0 \quad . \end{aligned} \quad (91)$$

The features of the spectra are:

- The neutronization peak consists of both, ν_e and ν_x fluxes, with the proportions determined by $\theta_\odot$ and P_H .
- The ν_e and $\bar{\nu}_e$ spectra are composite, with admixture of the hard component determined by the solar mixing angle.
- The ν_x spectrum contains components of all the three original spectra $(\nu_e, \bar{\nu}_e, \nu_x)$.

The earth matter effects can be significant for both the ν_e and $\bar{\nu}_e$ spectra. The effects on the ν_e spectrum are suppressed moderately by a factor of P_H.

Region III: Here $P_H \approx 1$, so that according to (88), $p \approx |U_{e2}|^2 \approx 0.2 - 0.4$. The H-resonance is inoperative, and the following transitions occur:

$$\nu_e \to \nu_2 \quad , \quad \nu_{\mu'} \to \nu_1 \quad , \quad \nu_{\tau'} \to \nu_3 \quad .$$

The features of the spectra are the same as those described in the case of the region II. Since $P_H \approx 1$, the earth matter effects are expected to be significant for both ν_e and $\bar{\nu}_e$ spectra.

Let us consider in some details the the earth matter effects which can give important signature of the scheme under consideration. For the ν_e spectrum the effect can be significant in regions II and III. Inserting $P_L = 0$ in (77), we get

$$F_e^D - F_e \approx P_H \cdot (P_{2e} - |U_{e2}|^2) \cdot (F_e^0 - F_x^0) \quad (92)$$

Using the constant density earth approximation (77) we estimate that the factor $(P_{2e} - |U_{e2}|^2)$ can be as large as 0.3 in the energy range of 20 – 50 MeV.

Similarly, for the antineutrinos, we get

$$F^D_{\bar{e}} - F_{\bar{e}} \approx (\bar{P}_{1e} - |U_{e1}|^2) \cdot (F^0_{\bar{e}} - F^0_x) \quad . \tag{93}$$

In the antineutrino channel, the effect can be significant in all three regions of U_{e3}, since there is no P_H suppression, and again the factor $(\bar{P}_{1e} - |U_{e1}|^2)$ can be as large as 0.3 for energies around 20–50 MeV.

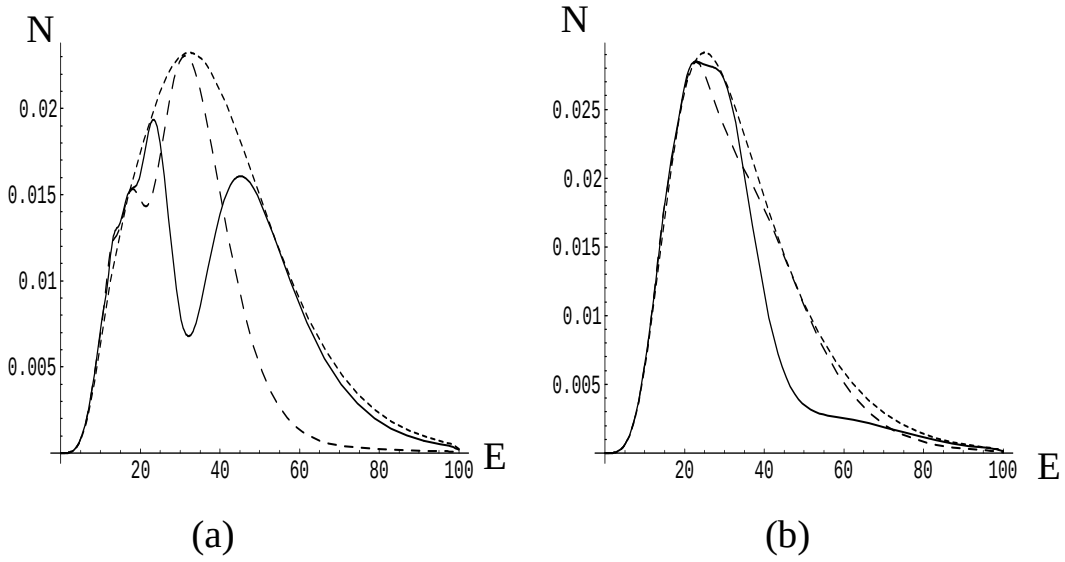

Figure 9: The earth matter effects on (a) the ν_e spectrum and (b) the $\bar{\nu}_e$ spectrum for $P_H = 1$ in the scheme with the LMA solution ($\Delta m^2 = 2 \cdot 10^{-5}$ eV^2, $\sin^2 2\theta_\odot = 0.9$). The dotted, dashed and solid lines show the spectra of the number of $\nu - N$ charged current events when the distance travelled by the neutrinos through the earth is $d = 0$ km, $d = 4000$ km, and $d = 6000$ km respectively.

In Fig. 9, we show the ν_e and $\bar{\nu}_e$ spectra for different distances travelled by the neutrinos through the earth. The sign of the earth effect (92, 93) is determined by the sign of $(F^0_e - F^0_x)$ in the neutrino channel and $(F^0_{\bar{e}} - F^0_x)$ in the antineutrino channel. The effect changes sign at $E = E_c$ ($E = \bar{E}_c$) for the neutrinos (antineutrinos), as described in Sec. 3.3 (Sec. 3.4). Since $P_{2e} \geq |U_{e2}|^2$ and $\bar{P}_{1e} \geq |U_{e1}|^2$, (92) and (93) imply that the earth effect results in the enhancement of neutrino (antineutrino) signal for $E < E_c$ ($E < \bar{E}_c$) and the depletion of the signal for $E > E_c$ ($E > \bar{E}_c$). Since the cross section of the neutrino detection interactions is larger at higher energies, a significant reduction in the ν_e ($\bar{\nu}_e$) flux is expected at energies greater than E_c ($\bar{E}_c$). It may manifest itself as a dip in the final spectrum (see Fig. 9), and this spectral distortion can indicate the presence of significant earth matter effects, even with the spectrum observed in only one detector.

4.3 The scheme with the VO solution

The mass and flavor spectrum for the scheme is shown in Fig. 10. The solar neutrino data is explained via the vacuum oscillations with $\Delta m^2 \sim 10^{-10}$ eV^2 and a large mixing between ν_e and a combination of ν_μ and ν_τ (5).

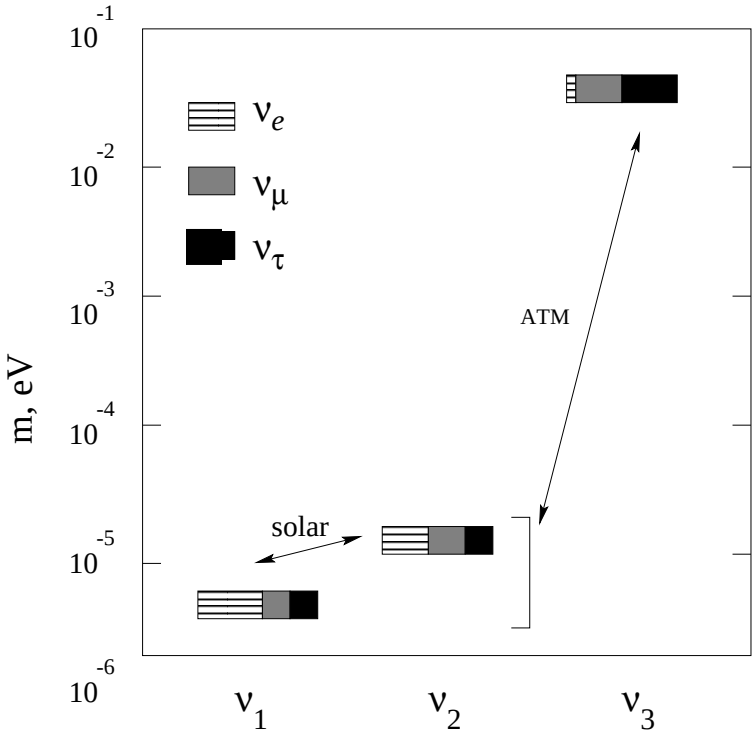

Figure 10: Neutrino mass and mixing pattern of the scheme with the vacuum osacillation solution for the solar neutrino data.

The level crossing scheme is shown in Fig. 5c, where the resonance L is close to $\rho = 0$. It may occur in the neutrino or antineutrino channel. Depending on the details of the density profile in the star at low densities, it lies either in the non-adiabatic region (so that $P_L, \bar{P}_L \approx 1$) or in the transition region.

Let us first consider the antineutrino channel. According to the level crossing scheme, we get the transitions

$$\bar{\nu}_e \to \bar{\nu}_1, \bar{\nu}_2 \quad , \quad \bar{\nu}_{\mu'} \to \bar{\nu}_1, \bar{\nu}_2 \quad , \quad \bar{\nu}_{\tau'} \to \bar{\nu}_3 \quad .$$

The final fluxes are given by (55) and for $\bar{p}$ we get from (60)

$$\bar{p} = \cos^2\theta_\odot(1 - \bar{P}_L) + \sin^2\theta_\odot \bar{P}_L \quad . \tag{94}$$

This implies that the value of $\bar{p}$ lies between $\cos^2\theta_\odot$ and $\sin^2\theta_\odot$, and the $\bar{\nu}_e$ spectrum is composite.

The fluxes in the neutrino channel depend on the region in which the oscillation parameters of the H resonance lie.

Region I. The H resonance is adiabatic, and the following transitions occur in the neutrino channel:

$$\nu_e \to \nu_3 \quad , \quad \nu_{\mu'} \to \nu_1, \nu_2 \quad , \quad \nu_{\tau'} \to \nu_1, \nu_2 \quad .$$

Since $P_H \approx 0$, from (55) we get

$$p \approx |U_{e3}|^2 \leq 0.03 \quad .$$

The ν_e then has the hard spectrum of the original ν_x. The observed features of the final fluxes are the same as those in the scheme with the LMA solution and an adiabatic H resonance (90). The earth matter effects are small for both the ν_e and $\bar{\nu}_e$ spectra, since the mixing angle $\bar{\theta}_{e2}$ is suppressed in the earth matter.

Region II. Jump probability in the H resonance is substantial, so that the transitions inside the star are:

$$\nu_e \to \nu_1, \nu_2, \nu_3 \quad , \quad \nu_{\mu'} \to \nu_1, \nu_2 \quad , \quad \nu_{\tau'} \to \nu_1, \nu_2, \nu_3 \quad .$$

From (55), we can infer

$$|U_{e3}|^2 \leq p \leq \cos^2\theta_\odot \quad . \tag{95}$$

where the lower bound corresponds to $P_H = 0$, whereas the upper bound is for $P_H = P_L = 1$. The ν_e spectrum is then composite.

The features of the spectra are:

- The neutronization peak should be observed both in ν_e and in ν_x channels.
- The $\bar{\nu}_e$ spectrum is composite, the admixture of the original hard component is determined by the solar mixing angle as well as by the degree of adiabaticity in the H and L conversion regions.
- The ν_e spectrum is composite, the admixture of the original hard component is determined by the solar mixing angle as well as the adiabaticity in the L resonance region.
- The ν_x spectrum contains components of all the three original spectra $(\nu_e, \bar{\nu}_e, \nu_x)$.

The earth matter effects are small for both the ν_e and the $\bar{\nu}_e$ spectra.

Region III. Since the H resonance is completely non-adiabatic, the neutrino transitions take place in L resonance region only:

$$\nu_e \to \nu_1, \nu_2 \quad , \quad \nu_{\mu'} \to \nu_1, \nu_2 \quad , \quad \nu_{\tau'} \to \nu_3 \quad .$$

From (55) we get for $P_H \approx 1$:

$$p \approx |U_{e1}|^2 P_L + |U_{e2}|^2(1 - P_L) \approx \cos^2\theta_\odot P_L + \sin^2\theta_\odot(1 - P_L) \quad . \tag{96}$$

Thus,

$$\sin^2\theta_\odot \leq p \leq \cos^2\theta_\odot \quad . \tag{97}$$

The ν_e - spectrum is composite. The features of the spectra are the same as those observed above in region II. The earth matter effects are small for both the ν_e and the $\bar{\nu}_e$ spectra.

The bi-maximal mixing scheme

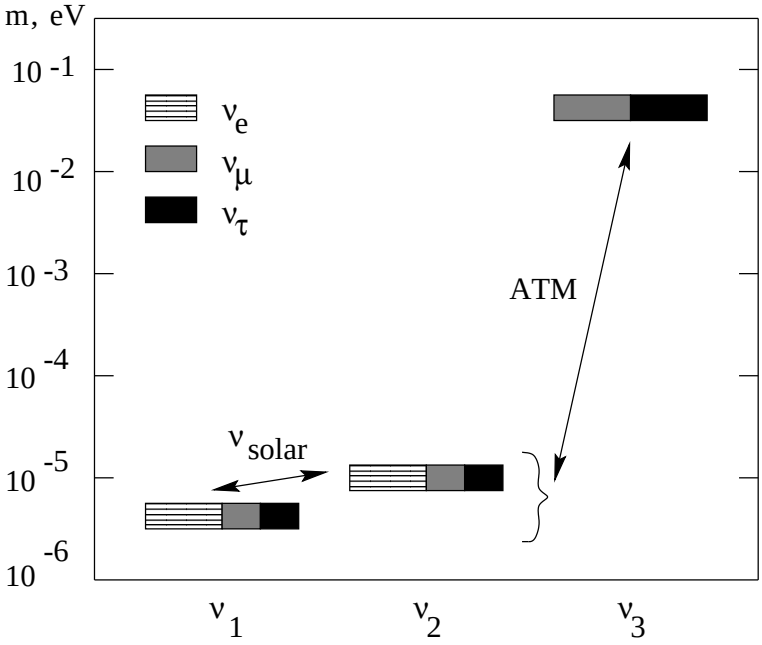

Figure 11: The neutrino mass and mixing pattern of the "strict" bimaximal mixing scheme.

An extreme case of the vacuum oscillations is the bimaximal mixing scenario [52]. The mass and flavor spectrum is as shown in Fig. 11. ν_μ and ν_τ mix maximally in $\nu_{\tau'} = (\nu_\mu + \nu_\tau)/\sqrt{2}$; in turn, the orthogonal combination $\nu_{\mu'} \equiv (\nu_\mu - \nu_\tau)/\sqrt{2}$ maximally mixes maximally with ν_e. In this scenario, $U_{e3} = 0$. The mass eigenstates are then

$$\nu_1 = (\nu_e - \nu_{\mu'})/\sqrt{2} \quad , \quad \nu_2 = (\nu_e + \nu_{\mu'})/\sqrt{2} \quad , \quad \nu_3 = \nu_{\tau'} \quad .$$

The following transitions take place:

$$\nu_e \rightarrow \nu_1, \nu_2 \quad , \quad \nu_{\mu'} \rightarrow \nu_1, \nu_2 \quad , \quad \nu_{\tau'} \rightarrow \nu_3 \quad ,$$
$$\bar{\nu}_e \rightarrow \bar{\nu}_1, \bar{\nu}_2 \quad , \quad \bar{\nu}_{\mu'} \rightarrow \bar{\nu}_1, \bar{\nu}_2 \quad , \quad \bar{\nu}_{\tau'} \rightarrow \bar{\nu}_3 \quad .$$

The mass eigenstates ν_1 and ν_2 ($\bar{\nu}_1$ and $\bar{\nu}_2$) arriving at the earth are observed with equal probability as electron or non-electron neutrinos. The expected fluxes are then

$$\begin{aligned} F_e &= (1/2)F_e^0 + (1/2)F_x^0 \quad , \\ F_{\bar{e}} &= (1/2)F_{\bar{e}}^0 + (1/2)F_x^0 \\ 4F_x &= (1/2)F_e^0 + 3F_x^0 + (1/2)F_{\bar{e}}^0 \quad . \end{aligned} \tag{98}$$

The neutrino spectra are affected in the following way:

- The neutronization peak consists of equal fractions of electron and non-electron neutrinos.
- The $\bar{\nu}_e$-spectrum is "composite", it has both the soft and the hard components in equal proportions.
- The ν_e-spectrum is also composite with both the soft and the hard components in equal portions. This spectrum has a lower average energy than the $\bar{\nu}_e$ spectrum, but the high energy tails of both the spectra are identical.
- The ν_x spectrum has a mixture of all the three initial spectra.

The earth matter effects are small for both ν_e and $\bar{\nu}_e$ spectra due to the small value of $\Delta m^2_{\odot} \sim 10^{-10}$ eV^2.

5 Conversion probabilities and neutrino fluxes with the inverted mass hierarchy

In the case of the inverted mass hierarchy (19), the mass eigenstates ν_1 and ν_2 are heavy and degenerate, whereas the third state ν_3 is much lighter: $m_1 \approx m_2 \gg m_3$. (see e.g. Fig. 12. for the scenario with the SMA solution).

As shown in Figs. 5b and 5d, the H-resonance is in the antineutrino channel, whereas the L-resonance lies in the neutrino channel for the SMA and LMA solutions. In the case of the VO solution, the L resonance can be in either the neutrino or the antineutrino channel.

Like in the case of the normal mass hierarchy, the fluxes at the earth can be written in terms of the survival probabilities p and $\bar{p}$ of ν_e and $\bar{\nu}_e$ respectively, as given in (64). Let us find the expressions for the survival probabilities p and $\bar{p}$.

As follows from the level crossing scheme (Figs. 5a and 5d), the matter eigenstates in the high density region ($\rho \gg \rho_H, \rho_L$) are

$$\nu_{1m} = \nu_{\mu'} \ , \ \nu_{2m} = \nu_e \ , \ \nu_{3m} = \nu_{\tau'} \ , \tag{99}$$

$$\bar{\nu}_{1m} = \bar{\nu}_{\tau'} \ , \ \bar{\nu}_{2m} = \bar{\nu}_{\mu'} \ , \ \bar{\nu}_{3m} = \bar{\nu}_e \ \ . \tag{100}$$

The state ν_e, which coincides with ν_{2m} in the production region, crosses the H-resonance layer adiabatically (since the resonance is in the antineutrino channel and the mixing in the neutrino channel is small), and reaches the L-layer as ν_{2m}. It reaches the surface of the earth as ν_1 with the probability P_L and as ν_2 with the probability $(1 - P_L)$. Then

$$p = |U_{e1}|^2 P_L + |U_{e2}|^2 (1 - P_L) \ \ . \tag{101}$$

The state $\bar{\nu}_e$, which coincides with $\bar{\nu}_{3m}$ in the production region, flips to $\bar{\nu}_{1m}$ in the resonance region H with the probability $\bar{P}_L$. Depending on the parameters of the solar neutrino solution, the propagation of the antineutrinos in the L-resonance region

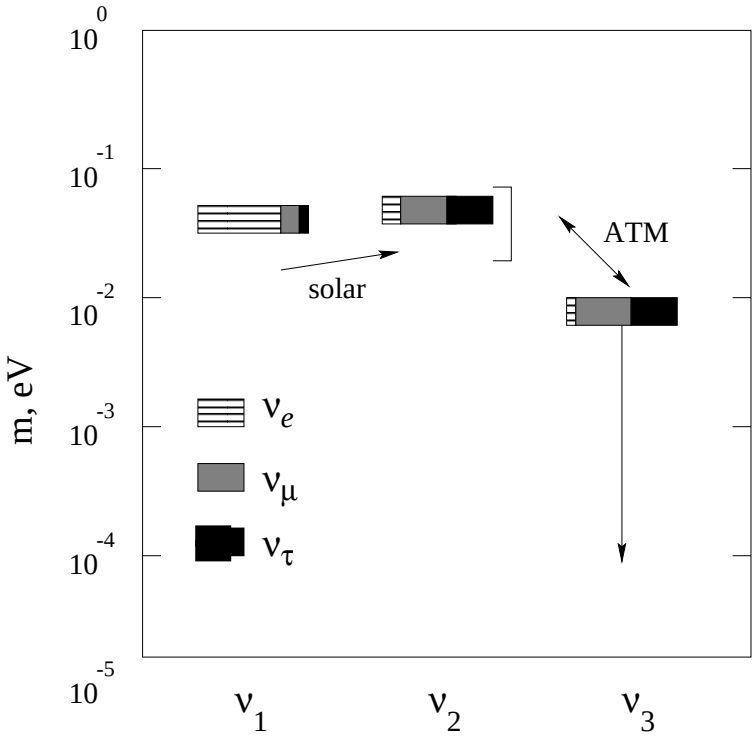

Figure 12: The neutrino mass and mixing pattern for the scenario with inverted mass hierarchy and the SMA solution for the solar neutrino problem.

(*i. e.* near $\rho = 0$) may or may not be adiabatic which is described by $\bar{P}_L$. Computing the probabilities of transitions of $\bar{\nu}_e$ to $\bar{\nu}_1$, $\bar{\nu}_2$, $\bar{\nu}_3$ and performing projection of the result back onto $\bar{\nu}_e$ back we get (similarly to (55) the survival probability $\bar{p}$ for the $\bar{\nu}_e$:

$$\bar{p} = |U_{e1}|^2 \bar{P}_H (1 - \bar{P}_L) + |U_{e2}|^2 \bar{P}_H \bar{P}_L + |U_{e3}|^2 (1 - \bar{P}_H) \quad . \tag{102}$$

(Here we have also averaged out the interference effects between the mass eigenstates, so that the three terms in (102) correspond to the three mass eigenstates.)

Let us consider the earth matter effects on the ν_e and $\bar{\nu}_e$ spectra for the inverted mass hierarchy. Since there is no H-resonance in the neutrino channel, the earth effects for the inverted hierarchy are the same as those described for the normal mass hierarchy (see Sec. 3.3) with $P_H = 1$:

$$F_e^{D1} - F_e^{D2} \approx (P_{2e}^{(1)} - P_{2e}^{(2)}) \cdot (1 - 2P_L) \cdot (F_e^0 - F_x^0) \quad . \tag{103}$$

The matter effects are significant for the scheme with the LMA solution. The suppression factor of P_H [that was present for the normal mass hierarchy - see eq. (75)] is now absent, so the earth matter effects can be larger than in the case of the normal mass hierarchy (see Fig. 9a).

The earth matter effects on the antineutrino spectra can be calculated as follows. Using the same arguments as for (102), we find the survival probability of $\bar{\nu}_e$ at the

detector:

$$\bar{p}^D = \bar{P}_{1e}\bar{P}_H(1-\bar{P}_L) + \bar{P}_{2e}\bar{P}_H\bar{P}_L + \bar{P}_{3e}(1-\bar{P}_H) \quad . \tag{104}$$

Then (102) and (104) give

$$\bar{p}^D - \bar{p} = (\bar{P}_{1e} - |U_{e1}|^2)(1-2\bar{P}_L)\bar{P}_H + (\bar{P}_{3e} - |U_{e3}|^2)(1-\bar{P}_H - \bar{P}_H\bar{P}_L) \quad , \tag{105}$$

where we have used $\sum \bar{P}_{ie} = 1$. Since $\bar{\nu}_3$ oscillates inside the earth with a very small depth [inequality (73) is valid with P_{3e} replaced by $\bar{P}_{3e}$], the second term in (105) can be neglected. Therefore, finally we get

$$F^{D1}_{\bar{e}} - F^{D2}_{\bar{e}} \approx \bar{P}_H(\bar{P}^{(1)}_{1e} - \bar{P}^{(2)}_{1e}) \cdot (1-2\bar{P}_L) \cdot (F^0_{\bar{e}} - F^0_x) \quad . \tag{106}$$

The earth matter effects on the $\bar{\nu}_e$ spectrum for the inverted hierarchy are then the same as those described for the normal hierarchy in Sec. 3.3, but further suppressed by a factor of $\bar{P}_H$. Significant effects can be observed only with the LMA scenario and when the H resonance is non-adiabatic.

The earth matter effects on both ν_e and $\bar{\nu}_e$ spectra are factorized, as in the case of the normal mass hierarchy. They are proportional to (i) the difference in original ν_e ($\bar{\nu}_e$) and ν_x fluxes, (ii) a factor which determines the conversion inside the star, and (iii) the difference of the oscillation probabilities inside the earth.

Notice that the expressions for the earth matter effects in inverted mass hierarchy case (103, 106) have the same form as the expressions in the normal hierarchy case (75, 80) with substitution: $\nu \leftrightarrow \bar{\nu}$, $P_H \leftrightarrow \bar{P}_H$.

Let us now calculate the values of the survival probabilities p and $\bar{p}$ for the three scenarios with the SMA, LMA and VO solutions for the solar neutrino problem respectively. Within each scenario, the final spectra would depend on the adiabaticity of antineutrino conversions in the H resonance layer, *i.e.* on the value of $|U_{e3}|^2$.

We shall consider the effects of neutrino conversions in three possible regions of $|U_{e3}|^2$: regions I, II and III as described in Sec. 2.5. When $|U_{e3}|^2$ lies in region III *i.e.* the H resonance is inoperative, the resulting final spectra for a given solar neutrino solution are the same as those obtained in Sec. 4.1, 4.2 and 4.3 for the normal mass hierarchy with the same mixing parameters. Therefore, we need to consider only the cases when $|U_{e3}|^2$ lies in regions I or II.

5.1 The scheme with the SMA solution

The characteristics of the ν_e spectrum are independent of the conversions at the H resonance layer [see eq. (101)]. The L resonance is in the transition region so that partial jumps from one level to another occur. As a consequence, from the level crossing scheme (Fig. 5b), we get the following transitions:

$$\nu_e \to \nu_1, \nu_2 \quad , \quad \nu_{\mu'} \to \nu_1, \nu_2 \quad , \quad \nu_{\tau'} \to \nu_3 \quad .$$

Neglecting terms proportional to the small $|U_{e2}|^2$ in (101), we get

$$p \approx P_L \quad .$$

The ν_e spectrum is thus composite.

Let us now examine the final $\bar{\nu}_e$ spectrum. Since the L resonance is in the neutrino channel, the antineutrino transitions in the L resonance layer are adiabatic, so that $\bar{P}_L \approx 0$. The characteristics of the final $\bar{\nu}_e$ spectrum depend on the region in which the value of $|U_{e3}|^2$ lies.

Region I. The following transitions take place inside the star:

$$\bar{\nu}_e \to \bar{\nu}_3 \quad , \quad \bar{\nu}_{\mu'} \to \bar{\nu}_2 \quad , \quad \bar{\nu}_{\tau'} \to \bar{\nu}_1 \quad .$$

For $P_H \approx 0$ the Eq. (102) gives

$$\bar{p} \approx |U_{e3}|^2 < 0.03 \quad .$$

The final $\bar{\nu}_e$ spectrum is then almost completely the original hard spectrum of ν_x:

$$F_{\bar{e}} \approx F_x^0 \quad .$$

The features of the final spectra are:

- The neutronization peak contains both, ν_e and ν_x fluxes.
- The ν_e and ν_x spectrua are composite.
- The $\bar{\nu}_e$ spectrum is practically the original hard spectrum of ν_x.

The earth matter effects on the ν_e spectrum (103) are small: $\lesssim 10\%$ (see Sec. 4.1), but still may be observable. The earth matter effects on the $\bar{\nu}_e$ spectrum (106) are negligible. They are suppressed by the factor of $\bar{P}_H \approx 0$ and further by the small mixing of the antineutrinos in the earth matter.

Region II. Taking into account jumps of states at H resonance we get the following transitions:

$$\bar{\nu}_e \to \bar{\nu}_1, \bar{\nu}_3 \quad , \quad \bar{\nu}_{\mu'} \to \bar{\nu}_2 \quad , \quad \bar{\nu}_{\tau'} \to \bar{\nu}_1, \bar{\nu}_3 \quad .$$

Inserting $\bar{P}_L \approx 0$ in eq. (102), we find

$$\bar{p} \approx \bar{P}_H \cos^2\theta_\odot \approx \bar{P}_H \quad .$$

The following features are then expected in the final spectra:

- The neutronization peak contains both ν_e and ν_x fluxes.
- All the three spectra, of ν_e, $\bar{\nu}_e$ and ν_x, are composite. In contrast with previous case (region I) now $\bar{\nu}_e$ spectrum is also composite.

The earth matter effects (103) are small: $\lesssim 10\%$ (see Sec. 4.1) for ν_e, and negligible for the $\bar{\nu}_e$.

5.2 The scheme with the LMA solution

The neutrino transitions at the L resonance are adiabatic, so that the following transitions take place according to the level crossing scheme (Fig. 5d):

$$\nu_e \to \nu_2 \quad , \quad \nu_{\mu'} \to \nu_1 \quad , \quad \nu_{\tau'} \to \nu_3 \quad .$$

Inserting $P_L \approx 0$ in Eq. (101), we get

$$p \approx |U_{e2}|^2 \approx \sin^2\theta_\odot \sim 0.2 - 0.4 \quad ,$$

and consequently, the ν_e spectrum is composite:

$$F_e \approx \sin^2\theta_\odot F_e^0 + \cos^2\theta_\odot F_x^0 \quad .$$

Let us examine the final $\bar{\nu}_e$ spectrum. The antineutrino transitions in the L resonance region are also adiabatic, so that $\bar{P}_L \approx 0$. Conversion in the H resonance region, and therefore the characteristics of the final $\bar{\nu}_e$ spectrum depend on $|U_{e3}|^2$.

Region I. Here the H resonance is adiabatic and we get the following transitions:

$$\bar{\nu}_e \to \bar{\nu}_3 \quad , \quad \bar{\nu}_{\mu'} \to \bar{\nu}_2 \quad , \quad \bar{\nu}_{\tau'} \to \bar{\nu}_1 \quad .$$

Since $P_H \approx 0$, the Eq. (102) gives

$$\bar{p} \approx |U_{e3}|^2 < 0.03 \quad .$$

and consequently, the $\bar{\nu}_e$ spectrum is then almost completely the original hard spectrum of ν_x:

$$F_{\bar{e}} \approx F_x^0 \quad .$$

The features of the final spectra are the same as those of the scheme with the inverted mass hierarchy and SMA solution (with $|U_{e3}|^2$ in region I). The earth matter effects on the ν_e spectrum (103) can be significant, as can be seen from Fig. 9a. In contrast, the earth effects on the $\bar{\nu}_e$ spectrum (106) are negligible: they are suppressed by the factor of $\bar{P}_H \approx 0$ and by the small mixing of the antineutrinos in the earth matter.

Region II. The transitions in the H resonance layer are incomplete and therefore according to the level crossing scheme we have

$$\bar{\nu}_e \to \bar{\nu}_1, \bar{\nu}_3 \quad , \quad \bar{\nu}_{\mu'} \to \bar{\nu}_2 \quad , \quad \bar{\nu}_{\tau'} \to \bar{\nu}_1, \bar{\nu}_3 \quad .$$

Inserting $\bar{P}_L \approx 0$ in eq. (102), we get

$$\bar{p} \approx \bar{P}_H |U_{e1}|^2 = \bar{P}_H \cos^2\theta_\odot \ .$$

The features of the final spectra are the same as those of the scheme with the inverted mass hierarchy and SMA solution (with $|U_{e3}|^2$ in region II). The earth matter effects can be significant both in the ν_e (103) and in the $\bar{\nu}_e$ channels (106) (see Fig. 9).

5.3 The scheme with the VO solution

The conversions in the H resonance layer does not influence ν_e flux. In the L resonance layer the adiabaticity is moderately broken: $P_L \neq 0$. From the level crossing scheme (Fig. 5d), the transitions taking place inside the star are:

$$\nu_e \to \nu_1, \nu_2 \quad , \quad \nu_{\mu'} \to \nu_1, \nu_2 \quad , \quad \nu_{\tau'} \to \nu_3 \quad .$$

From (101), we get

$$\sin^2\theta_\odot < p < \cos^2\theta_\odot \quad .$$

and since $\sin^2\theta_\odot > 0.3$ we get $p = 0.3 - 0.7$. The ν_e spectrum is thus composite.

Let us now examine the final $\bar{\nu}_e$ spectrum.

Region I. Due to adiabaticity in the H resonance layer, the following transitions take place:

$$\bar{\nu}_e \to \bar{\nu}_3 \quad , \quad \bar{\nu}_{\mu'} \to \bar{\nu}_1, \bar{\nu}_2 \quad , \quad \bar{\nu}_{\tau'} \to \bar{\nu}_1, \bar{\nu}_2 \quad .$$

Here $P_H \approx 0$, and from (102) we get

$$\bar{p} \approx |U_{e3}|^2 < 0.03 \quad .$$

The $\bar{\nu}_e$ spectrum is then almost completely the original hard spectrum of ν_x:

$$F_{\bar{e}} \approx F_x^0 \quad .$$

The features of the final spectra are similar to those of the scheme with the inverted mass hierarchy and SMA solution (with $|U_{e3}|^2$ in region I): the ν_e spectrum is composite whereas the $\bar{\nu}_e$ spectrum is purely hard. The earth matter effects on both ν_e and $\bar{\nu}_e$ spectra are negligible.

Region II. The adiabaticity is moderately broken both in the H and in the L resonance layers and the transitions proceed as

$$\bar{\nu}_e \to \bar{\nu}_1, \bar{\nu}_2, \bar{\nu}_3 \quad , \quad \bar{\nu}_{\mu'} \to \bar{\nu}_1, \bar{\nu}_2 \quad , \quad \bar{\nu}_{\tau'} \to \bar{\nu}_1, \bar{\nu}_2, \bar{\nu}_3 \quad .$$

Correspondingly the Eq. (102) gives

$$\bar{p} \approx \bar{P}_H[\cos^2\theta_\odot(1 - \bar{P}_L) + \sin^2\theta_\odot \bar{P}_L] \quad .$$

The features of the final spectra are the same as those of the scheme with the inverted mass hierarchy and SMA solution (with $|U_{e3}|^2$ in region II). The earth matter effects on both ν_e and $\bar{\nu}_e$ spectra are negligible.

Let us summarize the results. Some salient features of the final spectra with the inverted mass hierarchy are the following:

- The neutronization peak contains both ν_e and ν_x fluxes, in all the scenarios.
- Also the final ν_e spectrum is composite in all scenarios. The characteristics of this spectrum are independent of the oscillation parameters in the H resonance region.

- The final ν_x spectrum is composite in all scenarios.
- When the value of $|U_{e3}|^2$ lies in region I, the final $\bar{\nu}_e$ spectrum is almost the original hard spectrum of ν_x. For $|U_{e3}|^2$ in regions II and III the $\bar{\nu}_e$ spectrum is composite.
- The earth matter effects on the ν_e spectrum can be significant for the scheme with the LMA solution, marginally observable for the scheme with the SMA solution and negligible for the VO solution.
- The earth matter effects on the $\bar{\nu}_e$ spectrum can be significant only for the scheme with the LMA solution, and when the antineutrino transitions at the H resonance are not adiabatic. In all the other scenarios, the earth matter effects on $\bar{\nu}_e$ spectrum are negligible.
- When the value of $|U_{e3}|^2$ lies in region III, the final spectra (including the earth matter effects on them) are indistinguishable from those obtained with the scheme having the same oscillation parameters but the normal mass hierarchy.

6 Signals of mixing and signatures of mixing schemes

The future detection of a supernova neutrino burst by the underground neutrino detectors has been discussed in [53, 54, 55, 56]. For a typical supernova at 10 kpc, about 5000 $\bar{\nu}_e$ events are expected to be detected at SK, and a few hundred events each in SNO [57], LVD [58] and MACRO [59]. These detectors can reconstruct the energy of the outgoing charged lepton from the $\bar{\nu}_e - p$ charged current interactions. SK and SNO can also observe the direction of the charged lepton. In addition, SNO can detect ν_e and reconstruct its energy through the $\nu_e - d$ charged current interaction inside the D_2O. The feasibility of measuring the absolute values of the neutrino masses through the time-of-flight delays has been studied in [13, 60, 62]. Here, we concentrate on the features of the final neutrino spectra that are relevant for identification of the neutrino mass and flavor spectrum.

The effects of neutrino transitions on the final neutrino spectra can be observed through, *e.g.* (i) the partial or complete disappearance of the ν_e neutronization peak, (ii) the apperance of hard / composite spectra of ν_e or $\bar{\nu}_e$, (iii) earth matter effects. In this section, we shall elaborate on the effects that can be observed in the earth detectors.

6.1 The neutronization peak

The neutronization peak can be identified as the burst in the neutrino signal during the first few milliseconds. If there is no neutrino mixing, the neutrinos will be predominantly ν_e. Let the expected ratio of the number of charged current (CC) events to the number of neutral current (NC) events during the burst be

$$R_0^B \equiv \frac{N^{CC}}{N^{NC}} \quad .$$

If neutrino conversions transform some ν_e into ν_x, the number of charged current events decreases while the number of neutral current events remains unchanged. Then, the observed value of this ratio is $R^B < R_0^B$.

When the value of $|U_{e3}|^2$ lies in the region I in the case of the normal mass hierarchy (so that the neutrino transitions in the H resonance layer are adiabatic), the ν_e flux, and hence the number of charged current events, gets suppressed by a factor of $\approx |U_{e3}|^2$ (see Secs. 4.1, 4.2, 4.3):

$$\frac{R^B}{R_0^B} \approx |U_{e3}|^2 \leq 0.03 \quad . \tag{107}$$

The observation of $R_B > 0.03\ R_0^B$ would then point against $|U_{e3}|^2$ in region I for the normal mass hierarchy. According to (40), this will allow us to put an upper bound on the mixing parameter $|U_{e3}|^2$:

$$|U_{e3}|^2 \lesssim 3 \cdot 10^{-4} \quad . \tag{108}$$

6.2 The $\langle E \rangle$ inequalities and high energy "tails"

In the absence of mixing, one should observe $\langle E_{\nu_e} \rangle < \langle E_{\bar{\nu}_e} \rangle$. The inversion of this inequality, *i.e.* $\langle E_{\nu_e} \rangle > \langle E_{\bar{\nu}_e} \rangle$ is the signature of the ν-conversion. It implies that the contribution of the converted original hard ν_x spectrum to the final ν_e flux is significantly larger than its contribution to the final $\bar{\nu}_e$ flux.

In the case of the normal mass hierarchy, the inverted inequality for $\langle E \rangle$ will be observed when the transitions in the H resonance layer are adiabatic. The observation of the normal inequality $\langle E_{\nu_e} \rangle < \langle E_{\bar{\nu}_e} \rangle$ can exclude this scenario.

In the case of inverted mass hierarchy, the adiabatic transitions in the H resonance layer preserve the original inequalities for $\langle E \rangle$: $\langle E_{\nu_e} \rangle < \langle E_{\bar{\nu}_e} \rangle$. Therefore, an observation of the inequality $\langle E_{\nu_e} \rangle > \langle E_{\bar{\nu}_e} \rangle$ rules out the scenarios which have the inverted mass hierarchy with the value of $|U_{e3}|^2$ in region I. If the mass hierarchy is known to be the inverted one, an upper bound (108) on the mixing parameter $|U_{e3}|^2$ can be obtained.

The relative difference of the $\nu_e, \bar{\nu}_e$ and ν_x spectra is especially significant in the high energy ends ("tails") of the spectra, where the fluxes decrease exponentially with the increase of energy. In the absence of mixing, one expects

$$\frac{N_e(E > E_{tail})}{N_{\bar{e}}(E > E_{tail})} \ll 1, \quad \frac{N_{\bar{e}}(E > E_{tail})}{N_x(E > E_{tail})} \ll 1 \tag{109}$$

for high enough energy E_{tail} (energy greater than the peak energies of the spectra). Here $N_i(E > E_{tail})$ is the integrated number of $\nu_i - N$ charged current events above the energy E_{tail}.

The observation of the high energy ends of the ν_e and $\bar{\nu}_e$ spectra, where the contributions due to the original ν_e and $\bar{\nu}_e$ fluxes would be negligible, allows one to measure the contribution of the original hard ν_x spectrum to the final ν_e and $\bar{\nu}_e$ spectra.

Important conclusions can be drawn from the studies of the ratio

$$R(E_{tail}) \equiv \frac{N_e(E > E_{tail})}{N_{\bar{e}}(E > E_{tail})} \tag{110}$$

as E_{tail} increases.

1) $R(E_{tail}) \to \infty$:

This indicates that the tail of the ν_e spectrum extends to significantly higher energies than that of the $\bar{\nu}_e$ spectrum. This will testify for $\nu_e \leftrightarrow \nu_x$ conversions. Moreover, it will be a clear signal that the $\bar{\nu}_e \leftrightarrow \nu_x$ conversions are negligible, *i.e.* the $\bar{\nu}_e$ spectrum is the original soft spectrum. This would be an indication of (i) the SMA solution in the conventional hierarchy (sec. 4.1), or (ii) highly non-adiabatic H transitions with the SMA solution in the inverted hierarchy (sec. 5.1). If the mass hierarchy is known to be the inverted one, then this signal indicates that the value of $|U_{e3}|^2$ lies in region III. From (41), we obtain a very strong bound on the parameter $|U_{e3}|^2$:

$$4|U_{e3}|^2 \lesssim 10^{-5} \quad . \tag{111}$$

2) $R(E_{tail}) \to 0$:

Notice that the limit $R(E_{tail}) \to 0$ would be true in the absense of any neutrino conversion at all, or in the absence of conversion of the electron neutrinos. This situation is not realized in any of the scenarios we have discussed. The observation of $R(E_{tail}) \to 0$ would exclude all the scenarios under consideration and thus testify for the solution of the solar neutrino problem which differs from the MSW or VO solutions. Another possibility could be related to a compact star with a very sharp density profile, so that the L resonance is in the non-adiabatic region. In this case, the solar solution has to be SMA and the H resonance has to be inoperative for neutrinos.

3) $R(E_{tail}) \to const$:

This would testify for the contribution of the original ν_x to both final ν_e and $\bar{\nu}_e$ spectra. Moreover, the value of the constant will give us information about the mixing parameters.

In principle, the spectra of ν_x can be reconstructed by having a series of neutral current detectors with different thresholds. The ν_x spectrum will always have a dominating hard component. Therefore, the comparison of the high energy tails of the $\nu_e, \bar{\nu}_e$ with that of ν_x can directly give the measure of the hard component of the $\nu_e, \bar{\nu}_e$ spectra. The ability to measure the ν_x spectrum would also be useful in order to check for the presence of sterile neutrinos [9].

6.3 The identification of a composite spectrum

The final ν_e ($\bar{\nu}_e$) spectrum can be qualitatively divided into three types: (a) the original "soft" spectrum of the ν_e ($\bar{\nu}_e$) [corresponding to the survival probability $p = 1$ ($\bar{p} = 1$) which would be the case in the absence of conversion], (b) the "hard" original spectrum of ν_x [corresponding to the survival probability $p = 0$ ($\bar{p} = 0$) which would

be the case when there is a complete interchange of spectra], and (c) the "composite" spectrum, which is a mixture of the original soft and the hard spectra in comparable proportions.

In order to distinguish between (a) and (b), the values of "temperatures" (or average energies) of the original spectra need to be known, or the ν_e and $\bar{\nu}_e$ spectra have to be compared (as in Sec. 6.2). A composite spectrum may be identified without the knowledge of the initial temperatures and independently of the observation of the other spectrum, through the "broadening" phenomenon.

As described in Sec. 2.1, the instantaneous original neutrino spectra have a narrower energy distribution than the Fermi-Dirac one (see Fig. 1). The mixing between two neutrino species with different mean energies gives rise to an effective broadening of the spectrum (see Fig. 13), so that The final spectrum need not be pinched even though the two individual original spectra were pinched. In other words, the effective η for a mixed spectrum may be negative even though the individual η_i's of the constituent spectra were positive. The broadening of the spectrum can be checked by fitting the final spectrum with the parameters T_i and η_i (7) and establishing the sign of η_i.

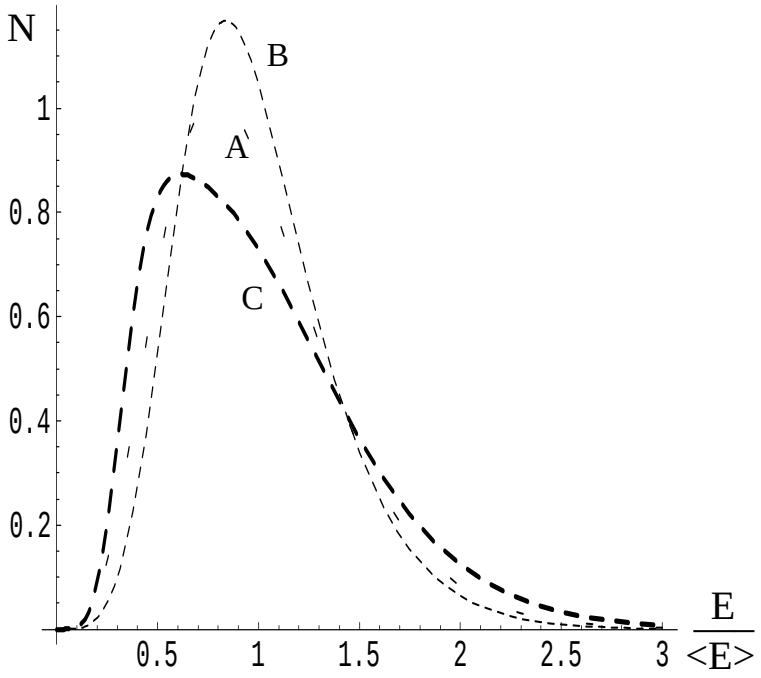

Figure 13: The number of $\nu - N$ charged current events for (A) a Fermi-Dirac spectrum ($T = 3, \eta = 0$): the solid line, (B) a pinched spectrum ($T = 3, \eta = 3$): the dotted line, and (C) a mixture of two pinched spectra ($T = 3, \eta = 3$ and $T = 8, \eta = 1$ with $E_{na} = 5$ MeV): the dashed line.

Note that the "pinching" phenomenon is established in a model independent manner only for a constant mean energy of the spectrum. A considerable variation in the average energy of neutrinos of a given species during the cooling phase could be responsible for the broadening of the time integrated spectrum even in the absence of

mixing. Therefore, in order to establish the broadening due to mixing, it is crucial to study the spectra in short intervals of time.

Clearly, it will be difficult to observe broadening of spectra, if the mean energies of the original spectra are very close, or if one of the original spectrum dominates in the final mixed spectrum.

The observation of broadening of the ν_e spectrum would point against an adiabatic H resonance in the normal hierarchy (see secs. 4.1, 4.2, 4.3). This would imply a strong upper bound (108) on the value of $|U_{e3}|^2$.

The observation of broadening of the $\bar{\nu}_e$ spectrum would be a strong indication against

- the SMA solution with the normal hierarchy (Sec. 4.1),
- completely adiabatic H transitions in the case of inverted hierarchy (secs. 5.1, 5.2, 5.3), and
- highly non-adiabatic H-transitions for the SMA solution with the inverted hierarchy (Sec. 5.1).

In particular, if the mass hierarchy is inverted, the broadening of $\bar{\nu}_e$ spectrum indicates that the H resonance is not completely adiabatic. This gives a strong upper bound (108) on $|U_{e3}|^2$.

If both the ν_e and $\bar{\nu}_e$ spectra are established to be composite, then the upper bound (108) on $|U_{e3}|^2$ holds irrespective of the type of mass hierarchy.

6.4 Earth matter effects

The earth matter effects can be observed through the comparison between the spectra at two detectors, or through the studies of the distortion of a spectrum in one detector (See Figs. 7, 9).

The earth matter effects are significant in the neutrino channel only in the cases of (i) normal mass hierarchy with the SMA or LMA scenario and a non-adiabatic H resonance, (ii) inverted mass hierarchy with the SMA or LMA scenario. In the antineutrino channels, significant earth matter effects are observed (sec. 3.4) only with (i) normal mass hierarchy with the LMA scenario, (ii) inverted mass hierarchy with LMA scenario and a non-adiabatic H resonance.

7 Identification of the mass spectrum

We show that with the 3ν schemes which explain the solar and atmospheric neutrino data, one can make rather reliable predictions of the conversion effects for supernova neutrinos. The predictions differ for different schemes, which opens up the possibility of discriminating among them using the data from the neutrino bursts.

We have studied the manifestation of the conversion effects in (i) The flavor composition of the neutronization peak: the main effect here is the partial or complete change of the flavor of the peak. This can be established by the comparison of the

			p	$\bar{p}$
I	SMA	normal	$\lvert U_{e3}\rvert^2$	1
		inverted	P_L	$\lvert U_{e3}\rvert^2$
	LMA	normal	$\lvert U_{e3}\rvert^2$	$\cos^2\theta_\odot$
		inverted	$\sin^2\theta_\odot$	$\lvert U_{e3}\rvert^2$
	VO	normal	$\lvert U_{e3}\rvert^2$	$[\sin^2\theta_\odot, \cos^2\theta_\odot]$
		inverted	$[\sin^2\theta_\odot, \cos^2\theta_\odot]$	$\lvert U_{e3}\rvert^2$
II	SMA	normal	$[\lvert U_{e3}\rvert^2, P_L]$	1
		inverted	P_L	$\bar{P}_H$
	LMA	normal	$\sin^2\theta_\odot P_H$	$\cos^2\theta_\odot$
		inverted	$\sin^2\theta_\odot$	$\cos^2\theta_\odot \bar{P}_H$
	VO	normal	$[\lvert U_{e3}\rvert^2, \cos^2\theta_\odot]$	$[\sin^2\theta_\odot, \cos^2\theta_\odot]$
		inverted	$[\sin^2\theta_\odot, \cos^2\theta_\odot]$	$[\sin^2\theta_\odot \bar{P}_H, \cos^2\theta_\odot \bar{P}_H]$
III	SMA	normal	P_L	1
		inverted	P_L	1
	LMA	normal	$\sin^2\theta_\odot$	$\cos^2\theta_\odot$
		inverted	$\sin^2\theta_\odot$	$\cos^2\theta_\odot$
	VO	normal	$[\sin^2\theta_\odot, \cos^2\theta_\odot]$	$[\sin^2\theta_\odot, \cos^2\theta_\odot]$
		inverted	$[\sin^2\theta_\odot, \cos^2\theta_\odot]$	$[\sin^2\theta_\odot, \cos^2\theta_\odot]$

Table 1: The values of the survival probabilities p and $\bar{p}$ for various scenarios. $[x, y]$ indicates that the value of the survival probability lies between x and y.

fluxes detected by charged current and neutral current interactions during the neutronization burst. (ii) Modifications of the ν_e and $\bar{\nu}_e$ spectra: Here one expects an appearance of hard or composite ν_e and/or $\bar{\nu}_e$ spectra due to mixing, instead of their original soft spectra. One can identify these effects of mixing by studying the average energies of spectra, the tails of spectra, and searching for the widening of the spectra. (iii) Earth matter effects: This can be done by detailed studies of the shapes of the energy spectra, or by the comparison of signals observed in different detectors.

The final spectra of ν_e and $\bar{\nu}_e$ can be characterized by the values of the survival probabilities p and $\bar{p}$ respectively. The conversion probabilities depend significantly on the value of $|U_{e3}|^2$. We have divided the whole range of possible values of $|U_{e3}|^2$ in three regions: I, II, and III, and have made definite predictions in each of these regions. Table 1 gives the values of the survival probabilities for the neutrino mass spectra under discussion.

The qualitative features of the final neutrino fluxes for various neutrino mass

			Neutronization peak	spectrum ν_e	spectrum $\bar{\nu}_e$	Earth effects ν_e	Earth effects $\bar{\nu}_e$
I	SMA	normal	$\approx \nu_x$	hard	soft	≈ 0	≈ 0
		inverted	$\nu_e,\ \nu_x$	composite	hard	$\surd$	≈ 0
	LMA	normal	$\approx \nu_x$	hard	composite	≈ 0	$\surd$
		inverted	$\nu_e,\ \nu_x$	composite	hard	$\surd$	≈ 0
	VO	normal	$\approx \nu_x$	hard	composite	≈ 0	≈ 0
		inverted	$\nu_e,\ \nu_x$	composite	hard	≈ 0	≈ 0
II	SMA	normal	$\nu_e,\ \nu_x$	composite	soft	$\surd$	≈ 0
		inverted	$\nu_e,\ \nu_x$	composite	composite	$\surd$	≈ 0
	LMA	normal	$\nu_e,\ \nu_x$	composite	composite	$\surd$	$\surd$
		inverted	$\nu_e,\ \nu_x$	composite	composite	$\surd$	$\surd$
	VO	normal	$\nu_e,\ \nu_x$	composite	composite	≈ 0	≈ 0
		inverted	$\nu_e,\ \nu_x$	composite	composite	≈ 0	≈ 0
III	SMA	normal	$\nu_e,\ \nu_x$	composite	soft	$\surd$	≈ 0
		inverted	$\nu_e,\ \nu_x$	composite	soft	$\surd$	≈ 0
	LMA	normal	$\nu_e,\ \nu_x$	composite	composite	$\surd$	$\surd$
		inverted	$\nu_e,\ \nu_x$	composite	composite	$\surd$	$\surd$
	VO	normal	$\nu_e,\ \nu_x$	composite	composite	≈ 0	≈ 0
		inverted	$\nu_e,\ \nu_x$	composite	composite	≈ 0	≈ 0

Table 2: The dependence of the final spectra on (1) the solution of the solar neutrino problem (2) the nature of hierarchy (normal or inverted) and (3) the value of $|U_{e3}|^2$. "Soft" in the ν_e column refers to the original ν_e spectrum and "soft" in the $\bar{\nu}_e$ column refers to the original $\bar{\nu}_e$ spectrum. "Hard" refers to the original ν_x spectrum. "Composite" implies that the final spectrum has both the soft and the hard components. In the Earth Matter Effects columns, a $\surd$ indicates the possibility of significant earth matter effects.

spectra, obtained in sec. 3-5, are summarized in Table 2. Let us first make some general observations from the table.

1. The complete disappearance of the ν_e neutronization peak (strong change of its flavor) and a pure hard spectrum of ν_e during the cooling stage always appear together. Their observation will testify for $|U_{e3}|^2$ in the region I and normal mass hierarchy, irrespective of the solution of the solar neutrino problem.

2. A pure hard $\bar{\nu}_e$ spectrum is the signature of the inverted mass hierarchy and $|U_{e3}|^2$ in the region I, irrespective of the solar neutrino solution.

3. A soft $\bar{\nu}_e$ spectrum can appear only in the schemes with the SMA solution of the solar neutrino problem.

4. The observation of any earth matter effects will rule out the scenarios with the VO solution.

5. The earth matter effects in $\bar{\nu}_e$ spectrum will be the signature of the LMA solution.

6. If the earth matter effects are observed in the neutrino channels but not in the antineutrino channels, we either have the normal mass hierarchy with $|U_{e3}|^2$ in regions II or III, or the inverted mass hierarchy.

7. If the earth matter effects are significant in both the ν_e and $\bar{\nu}_e$ channels, the solar neutrino solution is LMA and $|U_{e3}|^2$ lies in regions II or III.

Let us now systematically consider all the possible combinations of the observations. In general, the "observations" consist of the following features of the spectra:

- The flavor of the neutronization peak can be either mixed (ν_e, ν_x) or (almost) completely changed (ν_x).
- The ν_e spectrum at the cooling stage can be either hard or composite.
- The $\bar{\nu}_e$ spectrum can be of all possible types: soft (unchanged), hard, composite.
- The earth matter effects can be absent completely, or observed in one of channels (ν_e or $\bar{\nu}_e$), or observed in both channels.

The following conclusions can be drawn from the combinations of the above observations:

(A) Completely changed flavor (ν_x) of the neutronization peak, hard ν_e spectrum, and soft $\bar{\nu}_e$ spectrum. This configuration can be realized in only one case: normal hierarchy, SMA solution of the $\nu_\odot$-problem and $|U_{e3}|^2$ in the region I.

(B) Pure ν_x - neutronization peak, hard ν_e spectrum, and composite $\bar{\nu}_e$ spectrum. This implies normal mass hierarchy, $|U_{e3}|^2$ in the region I, and two possible $\nu_\odot$ solutions, LMA or VO. The observation of earth matter effects can distinguish between these two possibilities. For the LMA solution, the earth effects will be present in the $\bar{\nu}_e$ channel and absent in the ν_e channel.

(C) Mixed (ν_e, ν_x) flavor neutronization peak, composite ν_e spectrum, and soft $\bar{\nu}_e$ spectrum. This configuration can be realized in the three different cases: (i) SMA solution, normal mass hierarchy, and $|U_{e3}|^2$ in the region II, (ii) SMA solution, normal

mass hierarchy, but $|U_{e3}|^2$ in the region III, (iii) SMA solution, inverted hierarchy, $|U_{e3}|^2$ in the region III. Clearly such a configuration is the signature of the SMA solution of the $\nu_\odot$-problem. Earth matter effect is expected to be weaker in the case (i).

(D) Mixed (ν_e, ν_x) flavor neutronization peak, composite ν_e spectrum, composite $\bar{\nu}_e$ spectrum. This combination of observations can be realized in many cases: (i) SMA solution, inverted hierarchy, $|U_{e3}|^2$ in the region II, (ii-v) LMA solution, normal or inverted hierarchy, $|U_{e3}|^2$ in the regions II or III, (vi-ix) VO solution, normal or inverted hierarchy, $|U_{e3}|^2$ in the regions II or III. Studies of the earth effects can give an important criterion for discriminating between the above cases: they are absent in the VO cases (vi-ix) and should be observable in the ν_e channel but not in $\bar{\nu}_e$ channel in the SMA case (i). In the LMA case, the earth effects are expected both in the ν_e and $\bar{\nu}_e$ channels. Here a further discrimination can be done between (ii-v) by studying the degree of compositness: in the case of normal hierarchy one expects stronger effects in the neutrino channel.

(E) Mixed (ν_e, ν_x) flavor neutronization peak, composite ν_e spectrum, hard $\bar{\nu}_e$ spectrum. Such a combination of observations is realized with inverted hierarchy, $|U_{e3}|^2$ in the region I, and SMA or LMA or VO solution. That is, the combination does not depend on the solution of the $\nu_\odot$-problem and turns out to be the signature of the inverted mass hierarchy. In the cases with SMA or LMA solutions the earth effect can be observed in the ν_e channel only. No earth effect is expected in the VO case.

No other combination of the observables is realized in the mixing scenarios under disussion.

Establishing the region in which $|U_{e3}|^2$ lies is equivalant to giving bounds on the value of this mixing parameter, which correspond to the borders of the region. The borders depend on the precise density profile of the progenitor and can vary within a factor of 2 - 3. Thus, from SN data we can get bounds on $|U_{e3}|^2$ with an uncertainty of a factor of 2 - 3. In principle the value of $|U_{e3}|^2$ can also be measured (again within a factor of 2 -3) in the transition region where the effect (survival probability) depends substantially on U_{e3}.

The observations (A), (B), and (E) above establish $|U_{e3}|^2$ in region I, thus giving a lower bound of $|U_{e3}|^2 \gtrsim 3 \cdot 10^{-4}$. The observations (C) and (D) establish $|U_{e3}|^2$ to be in region II or III, thus giving an upper bound of $|U_{e3}|^2 \lesssim 3 \cdot 10^{-4}$. The upper bound obtained in the case of the observations (C) and (D) is more than an order of magnitude stronger than the one the long baseline experiments are planning to achieve. The observation of the broadening of both the ν_e and $\bar{\nu}_e$ spectra, or significant earth matter effects on both the ν_e and $\bar{\nu}_e$ spectra are sufficient to establish this bound.

A number of possible observations can rule out all the scenarios under discussion. The observation of (a) a pure ν_e neutronization peak and (b) a soft ν_e spectrum during the cooling stage is not possible with any of these neutrino mass spectra. The pairs of observations (a) pure ν_x neutronization peak and a composite ν_e spectrum, (b) mixed flavour neutronization peak and a pure hard ν_e spectrum, and (c) a hard

spectrum for both ν_e and $\bar{\nu_e}$ are also fatal for all the scenarios.

The final neutrino spectra can thus help in resolving three kinds of ambiguities that remain to be resolved with the current data: (i) the solution of the solar neutrino problem, (ii) the type of mass hierarchy (sign of Δm^2), and (iii) the value of $|U_{e3}|^2$.

The implications of results of this paper will depend on when neutrino burst from the Galactic supernova will be detected.

A number of results can be obtained from other experiments unrelated to the supernova neutrinos. Clearly, all the schemes considered above will be rejected if sterile neutrinos will be discovered in the oscillations of solar or atmospheric neutrinos, or if the LSND result will be confirmed. In this case, one will be forced to consider the schemes with sterile neutrinos [9].

On the other hand, there is a good chance that within several years the existing and future experiments will allow us to identify one of solutions of the solar neutrino problem considered in this paper. This will significantly diminish the number of possible schemes and will allow us to further sharpen the predictions of the effects for supernova neutrinos.

The purpose of this paper was to indicate the effects which can in principle testify for neutrino conversions and various features of the neutrino mass and flavor spectra. Clearly, further detailed studies are needed for specific detectors to clarify the detectability of the discussed effects and to conclude how far we can go in the program of identification of the neutrino mass spectrum.

Acknowledgements

One of us (A. D.) would like to thank J. Lattimer and G. Raffelt for discussions.

References

[1] Y. Fukuda et al., Phys. Rev. Lett. **82** (1999) 2644, K. Scholberg (for the SuperKamiokande collaboration), hep-ex/9905016.

[2] E. Peterson, for the SOUDAN 2 Collaboration, Nucl. Phys. Proc. Suppl. **77** (1999) 111.

[3] MACRO Collaboration, Talk by M. Spurio at 6th Topical Seminar on Neutrino and AstroParticle Physics, San Miniato, Italy, May 1999, hep-ex/9908066.

[4] M. Apollonio et. al., the CHOOZ collaboration, hep-ex/9907037.

[5] For global fits to the solar neutrino data, see e.g. J. N. Bahcall, P. I. Krastev and A. Yu. Smirnov, Phys. Rev. D **58** (1998) 096016. P. I. Krastev, hep-ph/9905458. M. C. Gonzalez-Garcia, P. C. de Holanda, C. Pena-Garay and J. W. F. Valle, hep-ph/9906469.

[6] G. L. Fogli, E. Lisi, D. Montanino and A. Palazzo, hep-ph/9910387

[7] D. White, for the LSND Collaboration, Nucl. Phys. Proc. Suppl. **77** (1999) 207.

[8] K. Eitel, hep-ex/9909036.

[9] A. S. Dighe and A. Yu. Smirnov, in preparation.

[10] L. Wolfenstein, Phys. Rev. D **17** (1978) 2369; Phys. Rev. D **20** (1979) 2634; S. P. Mikheyev and A. Yu. Smirnov, Sov. Phys. JETP, **64** (1986) 4; Sov. J. Nucl. Phys. **42** (1986) 913; Proc. of the 6th Moriond Workshop on Massive Neutrinos in Astrophysics and Particle Physics (Tignes, France), eds. O. Fackler and J. Tran Than Van, (1986) 355. G. M. Fuller et. al., Astroph. J. **322** (1987) 795. G. M. Fuller et. al., Astroph. J. **389** (1992) 517. G. Raffelt and G. Sigl, Astropart. Phys. **1** (1993) 165.

[11] J. Arafune et. al., Phys. Rev. Lett. **59** (1987) 1864. J. Arafune et. al., Phys. Lett. B **194** (1987) 477. P. O. Lagage et. al., Phys. Lett. B **193** (1987) 127. H. Minakata et. al., Mod. Phys. Lett. A **2** (1987) 827. S. P. Rosen, Phys. Rev. D **37** (1988) 1682. H. Minakata and H. Nunokawa, Phys. Rev. D **38** (1988) 3605.

[12] D. Nötzold, Phys. Lett. B **196** (1987) 315.

[13] P. Reinartz and L. Stodolsky, Z. Phys. C **27** (1985) 507.

[14] A. E. Chudakov, O. G. Ryazhskaya and G. T. Zatsperin, Talk given at the Denver 1973 Cosmic Ray Conference, Vol. 3 (1973) 2007. S. Choubey, D. Majumdar and K. Kar, J. Phys. G **25** (1999) 1001. D. Majumdar and A. Raychaudhuri, hep-ph/9901401.

[15] H. Athar, J. T. Peltoniemi and A. Yu. Smirnov, Phys. Rev. D **51** (1995) 6647.

[16] K. Fujikawa and R. E. Shrock, Phys. Rev. Lett. **45** (1980) 963.

[17] C. -S. Lim and W. J. Marciano, Phys. Rev. D **37** (1988) 1368. E. Kh. Akhmedov and Z. G. Berezhiani, in Les Arcs 1990, Proceedings, Particle astrophysics, pp. 305; Nucl. Phys. B **373** (1992) 479.

[18] G. C. McLaughlin, J. M. Fetter, A. B. Balantekin and G. M. Fuller, astro-ph/9902106.

[19] A. Yu. Smirnov, D. N. Spergel and J. N. Bahcall, Phys. Rev. D **49** (1994) 1389.

[20] K. S. Hirata et. al., Kamiokande collaboration, Phys. Rev. Lett. **58** (1987) 1490. R. M. Bionta et. al., IMB Collaboration, Phys. Rev. Lett. **58** (1987) 1494. E. N Alexeyev et. al, Pis'ma Zh. Eksp. Teor. Fiz. **45** (1987) 461 (JETP Lett. **45** (1987) 589.

[21] L. M. Krauss, Nature (London) **329** (1987) 689. J. A. Frieman, H. E. haber and K. Freese, Phys. Lett. B **200**, (1988) 115. A. E. Chudakov, Ya. S. Elensky and S. P. Mikheyev, Proc. of the NATO Advanced Study Institute, Erice, 1988. Kuwer Acad. Publ., eds. M. M. Shapiro and J. P. Wefel (1989) 131. B. Jegerlehner, F. Neubig and G. Raffelt, Phys. Rev. D **54** (1996) 1194.

[22] T. P. Walker and D. N. Schramm, Phys. Lett. B **195** (1987) 331.

[23] S. P. Mikheev and A. Yu. Smirnov, JETP Lett. **46** (1987) 10; Sov. Phys. Usp. **30** (1987) 759.

[24] T. K. Kuo and J. Pantaleone, Phys. Rev. D **37** (1988) 298.

[25] S. P. Mikheev and A. Yu. Smirnov, Prog. part. Nucl. Phys. **23** (1989) 41.

[26] T. K. Kuo and J. Pantaleone, Rev. Mod. Phys. **61** (1989) 937.

[27] F. Buccella et. al., Z. Phys. C **73** (1997) 633.

[28] A. Yu. Smirnov, Talk given at Symposium on New Era in Neutrino Physics, Tokyo, hep-ph/9811296.

[29] A. S. Dighe, Talk given at Valencia 99, International Workshop on particle Astrophysics and Cosmology: From Theory to Observation, May 1999, To be published in Proc. Suppl., Nucl. Phys. B.

[30] G. Dutta, D. Indumathi, M. V. N. Murthy and G. Rajasekaran, hep-ph/9907372.

[31] D.O. Caldwell, G.M. Fuller and Y.Z. Qian, astro-ph/9910175.

[32] For a comprehensive review of the astrophysical aspects of a Type II supernova burst, see H. Suzuki, Physics and Astriphysics of Neutrinos, eds. M. Fukugita and A. Suzuki, Springer-Verlag, 1994, pp. 763.

[33] C. J. Horowitz and G. Li, Phys. Lett. B **443** (1998) 58. S. Hannestad *et. al.*, astro-ph/9912242.

[34] E. S. Myra, J. M. Lattimer and A. Yahil, Supernova 1987A in the Large Magellanic Cloud, ed. M. Kafatos and A. Michalitsianos, Cambridge University Press, 1988.

[35] R. Mayle, J. R. Wilson and D. N. Schramm, Astroph. J. **318** (1987) 288.

[36] H. -T. Janka and W. Hillenbrandt, Astron. Astrophys. Suppl. **78** (1989) 375. H. -T. Janka and W. Hillenbrandt, Astron. Astrophys. **224** (1989) 49.

[37] G. Raffelt, Stars as Laboratories of Fundamental Physics, The University of Chicago Press, 1996.

[38] P. F. Harrison, D. H. Perkins and W. G. Scott, hep-ph/9702243; hep-ph/9904297.

[39] S. -H. Chiu and T. K. Kuo, hep-ph/9909461

[40] J. R. Wilson et. al., Annals of the New York Academy of Sciences, **470** (1986) 267.

[41] R. Mayle and J. R. Wilson, The Nuclear Equation of State, NATO Conf. Proc., Springer, Berlin, 1989. S. A. Colgate, Nature **341** (1989) 489.

[42] G. E. Brown, H. A. Bethe and G. Baym, Nucl. Phys. A **375** (1982) 481.

[43] L. Landau, Phys. Z. Sowjetunion **2** (1932) 46. C. Zener, Proc. R. Soc. London, Ser. A **137** (1932) 696.

[44] S. P. Mikheyev and A. Yu. Smirnov, Sov. J. Nucl. Phys. **42** (1985) 913; Yad. Fiz. **42** (1985) 1441.

[45] T. K. Kuo and J. Pantaleone, Phys. Rev. D **39** (1989) 1930.

[46] MINOS Technical Design Report, NuMI-L-337 TDR, October 1998.

[47] T. K. Kuo and J. Pantaleone, Phys. Rev. Lett. **57** (1986) 1805.

[48] F. J. Botella, C. S. Lim and W. J. Marciano, Phys. Rev. D **35** (1987) 896.

[49] H. -T. Janka, astro-ph/9503068.

[50] S. P. Mikheyev and A. Yu. Smirnov, in *Moriond 87*, Proceedings of the 7th Moriond Workshop on New and Exotic phenomena, Les Arcs, France, 1987, edited by O. Fackler and J. Trân Thanh Vân (Frontières, Paris, 1987), pp. 405. A.J. Baltz and J. Weneser, Phys. Rev. D **50** (1994) 5971; A.J. Baltz and J. Weneser, Phys. Rev. D **51** (1994) 3960; P. I. Krastev, hep-ph/9610339; Q.Y. Liu, M. Maris and S.T. Petcov, Phys. Rev. D **56** (1997) 5991; J.N. Bahcall and P.I. Krastev, Phys. Rev. C **56** (1997) 2839; M. Maris and S. T. Petcov, Phys. Rev. D **56** (1997) 7444.

[51] E. Kh. Akhmedov, Nucl. Phys. B **538** (1999) 25. E. Kh. Akhmedov, A. Dighe, P. Lipari and A. Yu. Smirnov, Nucl. Phys. B **542** (1999) 3.

[52] F. Vissani, hep-ph/9708483. V. Barger et. al., Phys. Lett. B **437** (1998) 107. A. Baltz, A. S. Goldhaber and M. Goldhaber, Phys. Rev. Lett. **81** (1998) 5730. H. Georgi and S. L. Glashow, hep-ph/9808293.

[53] T. Totani, K. Sato, H. E. Dalhed and J. R. Wilson, Astrophys. J. **496** (1988) 216.

[54] A. Burrows, D. Klein and R. Gandhi, Phys. Rev. D **45** (1992) 3361; Nuc. Phys. B (Proc. Suppl.) 31 (1993) 408.

[55] G. M. Fuller, W. C. Haxton and G. C. McLaughlin, Phys. Rev. D **59** (1999) 085005 and references therein.

[56] O. G. Ryazheskaya, V. G. Ryasny and O. Saavedra, JETP Lett. **56** (1992) 417; Nuovo Cim. **106 A** (1993) 257.

[57] J. Boger *et. al.*, SNO Collaboration, nucl-ex/9910016.

[58] M. Aglietta *et. al.*, LVD Collaboration, Nuovo Cim. **18 C** (1995) 629.

[59] M. Ambrosio *et. al.*, MACRO Collaboration, Astropart. Phys. **8** (1998) 123.

[60] J. F. Beacom and P. Vogel, astro-ph/9811350. P. Vogel, astro-ph/9904338. J. F. Beacom, hep-ph/9909231.

[61] M. Apollonio et. al., the CHOOZ collaboration, hep-ex/9906011.

[62] S. Choubey and K. Kar, hep-ph/9905327.